Check for updates

Chronic hyperglycemia impairs hippocampal neurogenesis and memory in an Alzheimer's disease mouse model

Elisabete Ferreiro [a,b], Mariagrazia Lanzillo [a], Diogo Canhoto [a,c],
António M. Carvalho da Silva [a,b], Sandra I. Mota [a,b], Inês S. Dias [a], Ildete L. Ferreira [a,b],
Ana R. Fontes [a], Giorgia Mastrella [a], Paulo Pinheiro [a,b], Jorge Valero [a,b,d,e,f],
A. Cristina Rego [a,c,*]

[a] CNC - Center for Neuroscience and Cell Biology, University of Coimbra, Coimbra, Portugal
[b] IIIUC-Institute for Interdisciplinary Research (IIIUC), University of Coimbra, Coimbra, Portugal
[c] Faculty of Medicine of the University of Coimbra (FMUC), Coimbra, Portugal
[d] Achucarro Basque Center for Neuroscience, Science Park of the University of the Basque Country (UPV/EHU), Leioa, Spain
[e] Ikerbasque - Basque Foundation for Science, Bilbao, Spain
[f] Department of Neurosciences, University of the Basque Country (UPV/EHU), Leioa, Spain

ARTICLE INFO

ABSTRACT

During aging, lifestyle-related factors shape the brain's response to insults and modulate the progression of neurodegenerative pathologies such as Alzheimer's disease (AD). This is the case for chronic hyperglycemia associated with type 2 diabetes, which reduces the brain's ability to handle the neurodegenerative burden associated with AD. However, the mechanisms behind the effects of chronic hyperglycemia in the context of AD are not fully understood. Here, we show that newly generated neurons in the hippocampal dentate gyrus of triple transgenic AD (3xTg-AD) mice present increased dendritic arborization and a number of synaptic puncta, which may constitute a compensatory mechanism allowing the animals to cope with a lower neurogenesis rate. Contrariwise, chronic hyperglycemia decreases the complexity and differentiation of 3xTg-AD newborn neurons and reduces the levels of β-catenin, a key intrinsic modulator of neuronal maturation. Moreover, synaptic facilitation is depressed in hyperglycemic 3xTg-AD mice, accompanying the defective hippocampal-dependent memory. Our data suggest that hyperglycemia evokes cellular and functional alterations that accelerate the onset of AD-related symptoms, namely memory impairment.

© 2020 Elsevier Inc. All rights reserved.

1. Introduction

Alzheimer's disease (AD) and type 2 diabetes (T2D) are age-related disorders that share common features: a disturbance in glucose metabolism and impaired insulin signaling (Sebastiao et al., 2014; Wijesekara et al., 2018). AD is the most prevalent neurodegenerative disease worldwide and is pathologically characterized by the presence of senile plaques and neurofibrillary tangles (Ferreira et al., 2010). Around 75% of AD patients develop T2D or glucose intolerance (Cowie et al., 2009; reviewed in Kroner, 2009). Metabolic alterations may occur early in the onset of AD, contributing to the development of the disease (Casadesus et al., 2007; Kroner, 2009). Besides, features of T2D, such as insulin resistance

and hyperglycemia, are associated with increased AD prevalence and thus considered risk factors for the disease (Wijesekara et al., 2018). In accordance, Carvalho et al. (2012) demonstrated that induction of a prediabetic state (by treating animals with 20% sucrose for 7 months) causes brain mitochondrial–related alterations and increases amyloid-β levels, 2 characteristics also observed in 11-month-old triple transgenic AD (3xTg-AD) mice, suggesting that diabetes is a risk factor for developing AD. Indeed, alterations in glucose metabolism affect brain function, its capacity to cope with insults (i.e., brain's cognitive reserve), hindering brain's functional compensation in age- or disease-related neuronal loss, accelerating the appearance of AD symptoms (Stern, 2009; Stranahan and Mattson, 2012).

The hippocampus constitutes a perfect region to analyze the brain's cognitive reserve in the context of AD. It is among the first brain structures to be affected by AD pathology (Gallagher and Koh, 2011), although it can constantly adapt to the cognitive demands of

* Corresponding author at: Center for Neuroscience and Cell Biology, University of Coimbra (polo 1), 1st Floor Fac. Medicine Building, Rua Larga, 3004-504 Coimbra, Portugal. Tel.: +351 239 820190; fax: +351 239 822776.
E-mail address: acrego@cnc.uc.pt (A.C. Rego).

the environment. This extraordinary adaptive capacity of the hippocampus relies mainly on its plastic synaptic activity, and its ability to produce adult-born neurons (neurogenic reserve) (Kempermann, 2008), which are reduced in AD patients (Moreno-Jiménez et al., 2019). The addition of a small number of neurons to the adult hippocampal circuitry at the level of the dentate gyrus (DG) critically influences memory processing. These newborn neurons present enhanced excitability and synaptic plasticity, which favor their recruitment into memory engrams and their action as key elements of DG signal filtering through the activation of local interneurons (Piatti et al., 2013; Rodríguez-Iglesias et al., 2019).

The neurogenic reserve is tightly modulated by lifestyle-related factors, such as exercise, stress, or diet, including hyperglycemia (Kempermann, 2008; Valero et al., 2016; Zainuddin and Thuret, 2012). Ultimately, life factors may exert an effect on intrinsic cellular and molecular pathways that control cell proliferation, survival, and differentiation (Valero et al., 2016). The canonical Wnt signaling pathway regulates target genes involved in neural stem cell proliferation and differentiation (Lie et al., 2005; Varela-Nallar and Inestrosa, 2013). Importantly, decreased β-catenin levels and impaired Wnt/β-catenin signaling may underlie altered adult hippocampal neurogenesis seen in the context of AD (Bayod et al., 2015; He and Shen, 2009; Tiwari et al., 2015), and also affect the formation of dendrites in newborn hippocampal neurons (Gao et al., 2007; Yu and Malenka, 2003).

Although many studies have revealed possible mechanisms behind the role of T2D in AD progression (de la Monte, 2012; Sebastiao et al., 2014), the influence of perturbed glucose metabolism on hippocampal neurogenesis has not been explored in the context of AD. Having this in consideration and the relevance of exploring the interaction between T2D and AD in the regulation of cognition, we explored a new possible link between T2D and AD progression by analyzing the effects of the perturbation of glucose metabolism, due to chronic hyperglycemia, on adult hippocampal neurogenic reserve and cognitive function in the triple transgenic AD (3xTg-AD) mice (a model with overexpression of human mutant amyloid precursor protein, presenilin-1, and microtubule-associated protein tau, causing neuropathological changes similar to those seen in AD patients). Our results strongly suggest that chronic hyperglycemia affects hippocampal neurogenesis and the capacity of the brain to cope with AD-like pathological burden, leading to defective learning and memory loss.

2. Materials and methods

2.1. Animals and ethics statement

Breeding pairs of homozygous 3xTg-AD mice harboring PS1/M146V, APPswe, and tauP301L transgenes, and respective non-transgenic (NonTg) control mice with the same genetic background (C57BL/6 × 129s), were kindly provided by Dr Frank LaFerla from the University of California, Irvine (Irvine, CA), which were genetically engineered as previously described (Oddo et al., 2003). Mice were bred and maintained at CNC-Faculty of Medicine animal house (license no. 520.000.000.2006, from the Portuguese animal welfare authorities). The development of amyloid and tau pathologies in males was confirmed in the CNC 3xTg-AD mouse colony, as shown in Mota et al. (2014). Two-month-old NonTg (n = 28) and 3xTg-AD (n = 25) male mice were used and randomly divided into 2 experimental groups: (1) untreated and (2) sucrose-treated animals. Mice were grouped in pairs in cages enriched with a malleable paper bag, handled every day and kept in the same room, under standard laboratory conditions: temperatures of 21 ± 2 °C, 12 hours light/dark cycle starting at 07:00 AM, ad libitum access to food (# 4RF21A; Mucedola, Milanese, Italy) and water, for untreated animals, or 20% sucrose for sucrose-treated mice. Investigators performing the experiments were blinded to the experimental groups. Animal weight and food consumption were monitored once a week, while liquid consumption was monitored every 2 days, simultaneously with bottle replacement (Supplementary Fig. 1). A pilot study was previously performed to estimate the period of sucrose treatment required to reach hyperglycemia and the adequate number of animals to be used. For the characterization of metabolic parameters, measurements were taken in the beginning of the light cycle, after a fasting period of 12 hours. A glucose tolerance test (GTT) was performed at 0, 3, and 6 months after beginning the sucrose treatment. Behavioral experiments were done during the dark cycle and these mice were fasted for 12 hours before sacrifice. All procedures were performed in order to minimize exposure to stress and suffering, in accordance with the approved animal welfare institutional guidelines (local welfare approval: ORBEA_140_2016/15072016; Directorate-General for Food and Veterinary [Direção-Geral de Alimentação e Veterinária] approval: 0421/000/000/2016) and European legislation (European directive 2010/63/EU).

2.2. Behavioral studies

The Morris water maze (MWM) test was performed in a circular pool (140 cm in diameter), surrounded with black curtains to which 4 different large white and black shapes were fixed (to serve as navigation cues). The pool was filled with water (21 ± 2 °C) and was rendered opaque by the addition of nontoxic white paint. For the training, a transparent platform (14 cm in diameter) was submerged 1 cm below the water surface. The room was maintained at a constant temperature of 25 °C and illuminated by a red light. A camera was fixed to the ceiling, above the pool center, and video recorded using the Debut video capture software v1.74 (NCH software; Greenwood Village CO). Mice were brought every day to the room 1 hour before the beginning of the experiments. Prior to training, mice were handled for 2 days. On the second day of handling, animals were briefly exposed (10 seconds) to the unsubmerged platform as a habituation protocol to facilitate posterior learning (Valero et al., 2014). Mice were then trained for 4 days with 6 trials per day. For each trial, mice were placed into the pool at one of the 4 predefined starting points in a pseudorandom order and allowed to search for the platform. Mice were guided to the platform if they were unable to reach it by themselves within 60 seconds. A minimum interval of 15 minutes was given to the animals between each trial. All animals with a thigmotaxia-like behavior during training were excluded from the study (only 3xTg-AD animals presented thigmotaxia, accounting for ~50% of 3xTg-AD mice). Memory retention was assessed by performing a probe test 24 hours after the last training trial, in which the animals were allowed to search for the absent platform for 60 seconds. Path analysis was performed using a custom-made macro for the Fiji software (Schindelin et al., 2012) (ImageJ 1.48v) and probe test parameters obtained using the Wintrack software (Wolfer et al., 2001). Data were expressed as mean (±standard error of the mean) for 8 untreated and 8 sucrose-treated NonTg mice, 4 untreated 3xTg-AD mice, and 6 sucrose-treated 3xTg-AD mice.

2.3. Immunofluorescence staining

Sixteen NonTg (8 untreated and 8 sucrose-treated) and 15 3xTg-AD (7 untreated and 8 sucrose-treated) mice were deeply anesthetized with sodium pentobarbital (70 mg/kg, i.p.). Immediately after blood collection by cardiac puncture, mice were perfused intracardially with 0.9% NaCl, for 4 minutes, by inserting the needle

through the ventricle into the ascending aorta. The brain was dissected out and the 2 hemispheres separated. One hemisphere was postfixed for 24 hours at 4 °C with 4% paraformaldehyde in phosphate-buffered saline (PBS; containing, in mM, 137 NaCl, 2.7 KCl, 1.8 KH₂PO₄, 10 Na₂HPO₄·2H₂O, pH 7.4), rinsed twice with PBS and cryoprotected with 30%(w/v) sucrose in PBS at 4 °C until it sank. Cryoprotected hemispheres were snap-frozen and kept at −80 °C. Left hemispheres were cut into 40-μm thick coronal sections using a cryostat-microtome (CM3050S; Leica, Mannheim, Germany). Slices were collected in 6 series and stored at −20 °C in antifreezing solution composed of 30% glycerol (v/v) and 30% polyethylene glycol (v/v) in 0.1 M phosphate buffer, pH 7.4.

For immunofluorescence staining, sections were rinsed in PBS overnight at 4 °C, and again 3× 10 minutes at room temperature (RT). For doublecortin (DCX) and Ki67 double staining, slices were left in blocking solution, composed of 3% bovine serum albumin (w/v) and 0.2% Triton X-100 in PBS, for 1 hour at RT. For DCX and postsynaptic density protein 95 (PSD95) double staining, slices were submerged in a blocking solution of 3% bovine serum albumin and 1% Triton X-100 in PBS. Sections were then incubated with primary antibodies prepared in their respective blocking solution for 72 hours, at 4 °C: goat anti-DCX (1:500; clone C-18, Sc-8066, RRID:AB_2088494, Lot #C0514, Santa Cruz Biotechnologies), rabbit anti-Ki67 (1: 2000; # ab16667, RRID:AB_302459, Lot # GR155005-2; Abcam, Cambridge, UK), mouse anti-PSD95 (1: 2000; clone K28/43, # MABN68, RRID:AB_10807979, Lot # 2424805; Merck Millipore), rabbit anti-β-catenin (1: 500; # ab32572, RRID:AB_725966, Lot # GR184212-3; Abcam), or chicken anti-microtubule associated protein 2 (1: 2000; # ab92434, RRID:AB_2138147; Abcam). Slices were then rinsed 3× 10 minutes with PBS and incubated for 2 hours at RT with the appropriate secondary antibodies diluted in PBS supplemented with Hoechst 33342 (0.2 μg/mL; # H1399; Thermofisher Scientific, Waltham, MA): Alexa Fluor 633 donkey antigoat immunoglobulin G (IgG) (# A21082, RRID:AB_10562400), Alexa Fluor 568 donkey antigoat IgG (# A11057, RRID:AB_2534104), Alexa Fluor 594 donkey antirabbit IgG (# A21207, RRID:AB_141637), Alexa Fluor 488 donkey anti-mouse IgG (# A21202, RRID:AB_141607), Alexa Fluor 488 donkey antirabbit IgG (#A-21206, RRID:AB_2535792), or Alexa Fluor 647 goat antichicken immunoglobulin Y (#A-21449, RRID:AB_2535866; all used at a dilution of 1:1000 and from Thermo Fisher Scientific). Sections were rinsed 3× 10 minutes with PBS and mounted with antifading medium (Fluoroshield Mounting Medium, # ab104135; Abcam).

2.4. Quantification of cell number and volume

The number of proliferating cells was estimated by counting Ki67-positive cells in the SGZ, and proliferating neuroblasts by identifying double-stained Ki67+ and DCX+ cells. All visible Ki67+ or Ki67+ and DCX+ cells were counted in slices separated by 240 μm, representing the entire DG (from bregma −4.04 mm to bregma −0.94 mm; Paxinos and Franklin, 1997), using a widefield fluorescence microscope (Axio Observer Z1; Zeiss), under a 40× oil immersion objective (NA 1.3). The total number of Ki67+ or Ki67+ and DCX+ cells was estimated by applying the Abercrombie formula (Petreanu and Alvarez-Buylla, 2002). Granular cell layer (GCL) area (from bregma −4.04 mm to bregma −0.94 mm) was measured based on the Hoechst 33342 staining in the DG by analyzing images obtained with a widefield fluorescence microscope (Axio Observer Z1, Zeiss; 20× magnification objective, NA 0.8), using the Fiji software (ImageJ 1.48v). The volume was estimated considering (1) that the irregular area of the DG in each tissue section may be reinterpreted as the area of a circle and thus (2) the volume of the DG between 2 consecutive measured sections is approximately

equivalent to the volume of a truncated cone whose base and top areas are equal to the areas of the 2 consecutively measured DG areas and the distance between them equals the height of the truncated cone. Therefore, we calculated the total volume of the DG as the sum of the volumes of the conical sections limited by each consecutive pair of measured sections. For this purpose, the areas of the sections were ordered from rostral to caudal and the volume calculated applying the mathematical formula $V = \pi \times h \times (R^2 + r^2 + R \times r)/3$, where V is the volume, h the height of the cone formed by the 2 sections (distance between the 2 slices), r the radius associated to the area of the DG of the first slice ($r = \sqrt{\frac{DGarea}{\pi}}$), and R the radius associated to the area of the DG of the second slice. Since slices were obtained in consecutive sections and only one of the 6 series was used, the volume of the rostral end of the GCL was calculated by estimating the radius of the most rostral section assuming the linear distribution of the area of the last 4 rostral sections.

DCX+ cells were counted using a widefield fluorescence microscope (Axio Observer Z1; Zeiss), under a 40× oil immersion objective (NA 1.3) in the GCL. The total number of cells was estimated as described above. Moreover, DCX+ cells were separated into 3 different groups based on dendritic morphology, as previously described (Plumpe et al., 2006). Briefly, DCX+ cells were separated into AB (cells with no processes or short ones), CD (cells with a medium process that may reach the molecular layer), and EF (cells with dendrites branching into the molecular layer or dendritic tree branching within the GCL) subgroups.

Average nuclear diameters of proliferating cells (Ki67+), proliferating DCX cells (Ki67+ and DCX+), neuroblasts (AB-DCX cells), differentiating neuroblasts (CD-DCX cells), and immature neurons (EF-DCX cells) were estimated by analyzing Hoechst 33342 staining in images captured with a widefield fluorescence microscope (Axio Observer Z1, Zeiss; 40× oil immersion objective [NA 1.3]; 0.4838 × 0.4838 × 1 μm [0.234 μm³] voxel size) using Fiji software.

2.5. Analysis of dendritic morphology

Three-dimensional (3D) reconstruction of dendritic trees from immature neurons was performed using confocal images obtained with an inverted Zeiss LSM 710 confocal microscope, equipped with a Plan-ApoChromat 40×/1.4 NA oil-immersion objective and a 0.7× digital zoom. Due to the sparse number of immature neurons in 3xTg-AD mice, images from all visible immature neurons were obtained in the DG, from bregma −4.04 mm to bregma −0.94 mm. Images from NonTg neurons were obtained by covering the same extension of the DG area used for 3xTg-AD analysis. 3D reconstruction was performed using the Simple neurite tracer plugin (Longair et al., 2011). A total of 110 (from 8 NonTg mice), 127 (from 8 sucrose-treated NonTg mice), 40 (from 7 3xTg-AD mice), and 22 (from 4 sucrose-treated 3xTg-AD mice) cells were reconstructed. Immature neurons were separated into short (cells that do not reach the outer and medial molecular layer [O/MML]) or long (cells that reach the O/MML) EF-DCX cells. Cell type classification was obtained using the average DG IML and O/MML thickness per animal. IML and O/MML average thicknesses were obtained based on PSD95 staining (more intense in the IML) in all DG slices/animal using a widefield fluorescence microscope (Axio Imager Z2 system; Zeiss) and the Stereo Investigator software. Dendritic morphology was analyzed using the 3D Sholl analysis Fiji plugin (http://fiji.sc/Sholl_Analysis) by quantifying the number of intersections between dendrites and the surface of spheres with a radius increment of 10 μm. Complexity and length of dendrites were further analyzed with the ImageJ plugins Skeletonize3D (https://imagej.net/Skeletonize3D) and AnalyzeSkeleton (https://imagej.net/AnalyzeSkeleton).

2.6. Quantification of PSD95 puncta

The number of PSD95-positive puncta, corresponding to putative sites of synaptic contact, were analyzed in confocal image stacks taken with an inverted Zeiss LSM 710 confocal microscope, equipped with a Plan-ApoChromat 63×/1.4 NA oil-immersion objective and a 5× digital zoom (QUASAR detection unit; ZEN Black software). Three-plane confocal images (0.053 × 0.053 × 0.7 μm [0.00197 μm³] voxel size for an image size of 26.99 × 26.99 × 0.9 μm [665.61 μm³]) of regions with homogenous punctuate PSD95 signal were acquired in the DG suprapyramidal IML or O/MML (n = 35/38, 43/44, 31/30, and 19/25 IML/O/MML images for NonTg [8 mice], sucrose-treated NonTg [8 mice], 3xTg-AD [7 mice], and sucrose-treated 3xTg-AD groups [4 mice], respectively, acquired from bregma −3.4 mm to bregma −1.34 mm). Before PSD95 puncta quantification confocal images were deconvolved using Huygens Essential software (Scientific Volume Imaging, Hilversum, The Netherlands) and a theoretical point spread function. A custom-made macro for the Fiji software (ImageJ 1.48v) was programmed to process the confocal images and automatically quantify PSD95 puncta. This macro allowed the sequential use of several image filters namely background normalization (subtract background, http://imagejdocu.tudor.lu/doku.php?id=gui:process: subtract_background), puncta segmentation ("FindFoci" plugin; Herbert et al., 2014), and stereological selection of puncta (Vamp3D plugin; Dumitriu et al., 2012). For puncta quantification in DCX+ dendrites, regions of interests delimiting portions of DCX-positive apical dendrites were drawn (n = 274/277, 223/177, 203/196, 102/ 100 dendrites segments in the IML/O/MML for NonTg, sucrose-treated NonTg, 3xTg-AD, and sucrose-treated 3xTg-AD groups, respectively) and the number of puncta per dendritic length (puncta/μm) calculated. The total number of PSD95 puncta in EF-DCX cells was then estimated using the total length of DCX dendrites obtained during the analysis of dendritic morphology. Only puncta with more than 50% colocalization with dendrites were included in the quantification. Quantification of the number of PSD95 puncta/μm³ (puncta density) in the IML and O/MML was performed in confocal image stacks. Estimation of the total puncta number (Supplementary Fig. 5) was performed using PSD95 puncta density, and IML and O/MML volumes previously quantified (Supplementary Fig. 6). The custom-made macro also allowed the quantification of average puncta size.

2.7. Quantification of β-catenin levels

β-Catenin levels were quantified in single-plane confocal images obtained using an inverted Zeiss LSM 710 confocal microscope, equipped with a Plan-ApoChromat 40×/1.4 NA oil-immersion objective (105 [n = 11–16/animal; 8 mice], 104 [n = 10–15/animal; 8 mice], 72 [n = 9–17/animal; 7 mice], and 82 [n = 5–15/animal; 7 mice] images for untreated/sucrose-treated NonTg and untreated/sucrose-treated 3xTg-AD groups, respectively, from −3.52 mm to bregma −1.34 mm). Confocal images were analyzed using the Fiji software (ImageJ 1.51f). An ImageJ macro was designed to create selections of the nuclei and somata of neuroblasts and immature neurons of the DG GCL, as well as the nuclei of mature neurons of DG GCL. A second macro was then developed to subtract the nucleus selection from the soma selection to obtain a selection corresponding to the cytoplasm of neuroblasts and immature neurons. Mature neurons are abundant in the DG GCL and located in close proximity, thereby making it impossible to delineate their somata as done in the neuroblasts and immature neurons. To circumvent this problem, another macro was used to create a 6-pixel-wide cytoplasm band selection around the nucleus. A final macro was designed to quantify the single-cell mean integrated density of β-catenin signals, determined at all possible thresholds, and divided by the respective area (published in Matos et al., 2016, with some modifications). Results are presented as the area under the curve of the first 5 thresholds (corresponding to the maximum intensity of β-catenin signal) of 54/60 or 89/81 cells in untreated/sucrose-treated 3xTg-AD or NonTg neuroblasts, respectively; 31/22 or 98/117 cells in untreated/sucrose-treated 3xTg-AD or NonTg immature neurons, respectively; and 256 cells per group for mature neurons.

2.8. Electrophysiology

Twelve (6 untreated and 6 sucrose-treated) NonTg and 9 (4 untreated and 5 sucrose-treated) 3xTg-AD mice were used. The mice were deeply anesthetized with sodium pentobarbital (70 mg/ kg i.p.) and transcardially perfused with oxygenated (95% O_2, 5% CO_2), ice-cold artificial cerebrospinal fluid (ACSF) composed of (in mM): 119 NaCl, 2.3 KCl, 1.3 $MgSO_4$, 2.5 $CaCl_2$, 26.2 $NaCHO_3$, 1 NaH_2PO_4, and 11 glucose. The brains were rapidly removed and 300 μm sagittal slices from the left hemisphere were cut using a vibratome (Leica VT1200S). The slices were transferred to a recovery chamber containing oxygenated ACSF at 32 °C for 30 minutes and then stored at RT for a minimum of 1 hour before starting the recording. Slices were then placed in a recording chamber and perfused with oxygenated ACSF at 32 °C and a flow rate of ~2 mL/ min. Evoked field potentials were recorded in the outer molecular layer of the DG, close to the hippocampal fissure, using glass microelectrodes filled with 4M NaCl (1–2 MΩ of tip resistance). The lateral perforant pathway (LPP) was stimulated using an isolated stimulation unit (Digitimer) and a concentric bipolar electrode (FHC). Only recordings displaying paired-pulse facilitation (50 ms interpulse interval) were accepted. Input-output curves were obtained after 10 minutes of stable recordings and, due to the small size of field excitatory postsynaptic potentials (fEPSPs), a stimulation intensity producing 50%–60% of the maximal response was used for both test pulses and tetanus. Test pulses were delivered every 20 seconds for 15 minutes for obtaining a baseline recording and long-term potentiation (LTP) was induced using 1 second 100 Hz trains of stimulation, repeated 4 times with a 15 seconds interval. Subsequently, responses were registered every 20 seconds for up to 50 minutes following the high-frequency stimulation (HFS). The signals were acquired using an HEKA EPC10 double amplifier and the Patchmaster software, filtered at 2.9 kHz and sampled at 10–20 kHz. Amplitude measurements were used for input-output curves and normalized fEPSP slopes were used to calculate changes in synaptic efficacy following HFS. The change in synaptic efficacy was evaluated between 30 and 40 minutes after HFS.

2.9. Principal component analysis

Principal component analysis (PCA) was performed using the software Past4.0. As variables were measured in different units, we used the correlation option that normalizes all variables by dividing them by their standard deviations. Iterative computation was used to handle missing values (Ilin and Raiko, 2010). PCA data (eigenvalues, % of variance, scores, and loadings) are provided in the Supplementary data file "Suppl PCA data.xlsx."

2.10. Statistical analysis

The number of animals used is mentioned in the Materials and methods section and each figure caption. Statistical tests used are also mentioned in each figure caption. Data are expressed as mean ± standard error of the mean, with points indicating

individual values when the *N* was inferior to 8. For *N* > 8, individual values were not included for clarity purposes. Statistical significance was determined using 2-way analysis of variance (ANOVA) followed by Bonferroni post hoc test performed using GraphPad Prism v7 (San Diego, CA). Repeated measures ANOVA or factorial ANOVA (for multiple factors), followed by Bonferroni post hoc test, were performed using SPSS 23 for Windows (SPSS Inc, Chicago, IL). *p*-values <0.05 were considered statistically significant. For correlations, normality of the data was first evaluated using the D'Agostino & Pearson omnibus normality test performed using GraphPad Prism v7. For data without normal distribution, a nonparametric Spearman correlation was used. For those that passed normality tests, Pearson correlation coefficients were applied instead.

The computer code and data produced in this study can be obtained from the corresponding author, upon reasonable request.

3. Results

3.1. Spatial memory is compromised in hyperglycemic

3.1.1. 3xTg-AD mice

To study whether hyperglycemia may affect the neurogenic reserve and accelerate the appearance of AD-related symptoms, we analyzed the effect of chronic hyperglycemia on hippocampal neurogenesis and memory in 8-month-old 3xTg-AD mice. We induced hyperglycemia in 3xTg-AD and NonTg mice by treating them for 6 months with 20% sucrose in the drinking water (Supplementary Table 1 and Supplementary Fig. 1). Sucrose-treated mice displayed glucose intolerance, as shown by the oral GTT (Supplementary Fig. 1 and Supplementary Table 1), indicating the development of a hyperglycemic phenotype.

Cognitive function in hyperglycemic 3xTg-AD mice was evaluated at the end of the 6 months of sucrose treatment by analyzing spatial learning and memory with the MWM test (Fig. 1). As expected, untreated 8-month-old NonTg mice learned the MWM task (Fig. 1A) and formed long-term memory of the position of the submerged platform (Fig. 1B–F). Hyperglycemic NonTg mice showed no difference in learning and memory capacity when compared to their age-matched controls (Fig. 1). During the acquisition phase, 3xTg-AD mice revealed a less efficient learning pattern compared to NonTg controls (Fig. 1A), indicating a defective learning capacity. Nonetheless, the probe test data revealed that 3xTg-AD mice had some capacity to retain the localization of the hidden platform (Fig. 1B–D). However, hyperglycemia totally impairs spatial memory as indicated by the number of platform crossings, the time spent in the target quadrant, and the average distance to the platform (Fig. 1B–D). In agreement with these data, a significant increase in the cumulative search error (which accounts for the efficiency of the search strategy), was observed in hyperglycemic 3xTg-AD mice (Fig. 1E). During the probe test, the increase in the average distance traveled to reach the platform (path length) positively correlated with the level of glucose intolerance in 3xTg-AD mice, but not in NonTg mice (Fig. 1G). Neither 3xTg-AD genotype nor chronic hyperglycemia affected mouse swimming ability (Supplementary Fig. 2). These results show that chronic hyperglycemia induces cognitive deficits specifically in 3xTg-AD mice.

3.2. Chronic hyperglycemia decreases the complexity of immature DCX+ neurons in 3xTg-AD mice

Adult neurogenesis is a specific form of brain plasticity, with functional relevance for pattern separation and spatial learning (Garthe and Kempermann, 2013; Kempermann, 2008). Given that

hyperglycemia induced spatial memory impairment in 3xTg-AD mice, we hypothesized that adult neurogenesis could be also affected in these mice. Hence, we evaluated both the proliferation and the number of neuronal precursors and maturing neurons in the GCL of the DG. The extent of proliferation was determined by counting the number of cells expressing the proliferation marker Ki67, which is found in all phases of the active cell cycle of proliferating cells (G1, S, G2, and M) (Bologna-Molina et al., 2013) (Fig. 2). Chronic hyperglycemia significantly increased (by ~1.7-fold) the number of proliferating cells (Ki67+ cells) in the GCL of both NonTg and 3xTg-AD mice, when compared to their age-matched controls (Fig. 2B), demonstrating that hyperglycemia promotes cell proliferation. During adult neurogenesis, the proliferation of transit amplifying progenitor cells and neuroblasts strongly contributes to the final number of newly generated neurons (Kempermann et al., 2004). Since DCX, a cytoskeletal-related molecule, is only expressed in early neuroblasts and up to 28 days in rodent neurons (Encinas et al., 2011; Plumpe et al., 2006), neuroblast proliferation was evaluated by counting the number of cells co-expressing DCX and Ki67 (Fig. 2C). Sucrose treatment induced a significant increase in the total number of Ki67+ and DCX+ cells in the GCL. Although post hoc analysis showed no significant differences, a tendency for increased number of Ki67+ and DCX+ cells was evident in sucrose-treated NonTg and 3xTg-AD mice, when compared to their respective controls (Fig 2C).

We next quantified the different cell types that constitute the DCX-positive cell population, namely neuroblasts, differentiating neuroblasts and immature neurons (AB-, CD-, and EF-DCX+ cells, respectively), based on their different morphologies (Plumpe et al., 2006). The number of the 3 different DCX+ cell types was significantly reduced in the GCL of 3xTg-AD when compared to NonTg mice. This confirms our previous data indicating reduced incorporation of newborn neurons in the hippocampus of 3xTg-AD mice (Valero et al., 2014). However, and despite the increase in DCX+ cell proliferation induced by our sucrose treatment (Fig. 2B and C), hyperglycemic 3xTg-AD mice did not show any significant increase in DCX+ neuroblasts (AB cells), while hyperglycemic NonTg mice showed a moderate increase (Fig. 2E).

The degree of morphological complexity of the dendritic trees of immature neurons is essential since it relates to the probability of the cell to adequately integrate into the hippocampal circuitry, through the establishment of contacts with perforant path fibers coming from the entorhinal cortex (EC), allowing the information to be conveyed to cornu ammonis area 3 (Piatti et al., 2013). EF-DCX cells were 3D-reconstructed and the Sholl analysis used to evaluate the complexity of their dendritic trees. EF-DCX cells from 3xTg-AD mice that reached the O/MML showed increased dendritic complexity specifically in the O/MML (radius 140–170 μm) (Fig. 3B). This was also reflected by a significant increase in the number of dendritic branches and branch junctions in EF-DCX cells from 3xTg-AD mice, when compared to NonTg mice (Fig. 3D). Interestingly, the dendrites of newly generated neurons from sucrose-treated 3xTg-AD mice presented a totally different morphological pattern, with increased complexity in the GCL, highly reduced ramifications in the ML (radius 80–150 μm), and decreased number of dendritic branches and junctions (Fig. 3B and D) when compared to untreated 3xTg-AD mice. Nevertheless, no overall alterations were found in total dendritic length and volume in immature neurons from hyperglycemic 3xTg-AD mice (Fig. 3C). Importantly, a strong negative correlation between the number of dendritic branches located in the O/MML and the degree of glucose intolerance was found exclusively in newly generated neurons from 3xTg-AD mice (Fig. 3E). Interestingly, the dendritic complexity of EF-DCX+ cells that did not reach the O/MML decreased specifically in the ML in
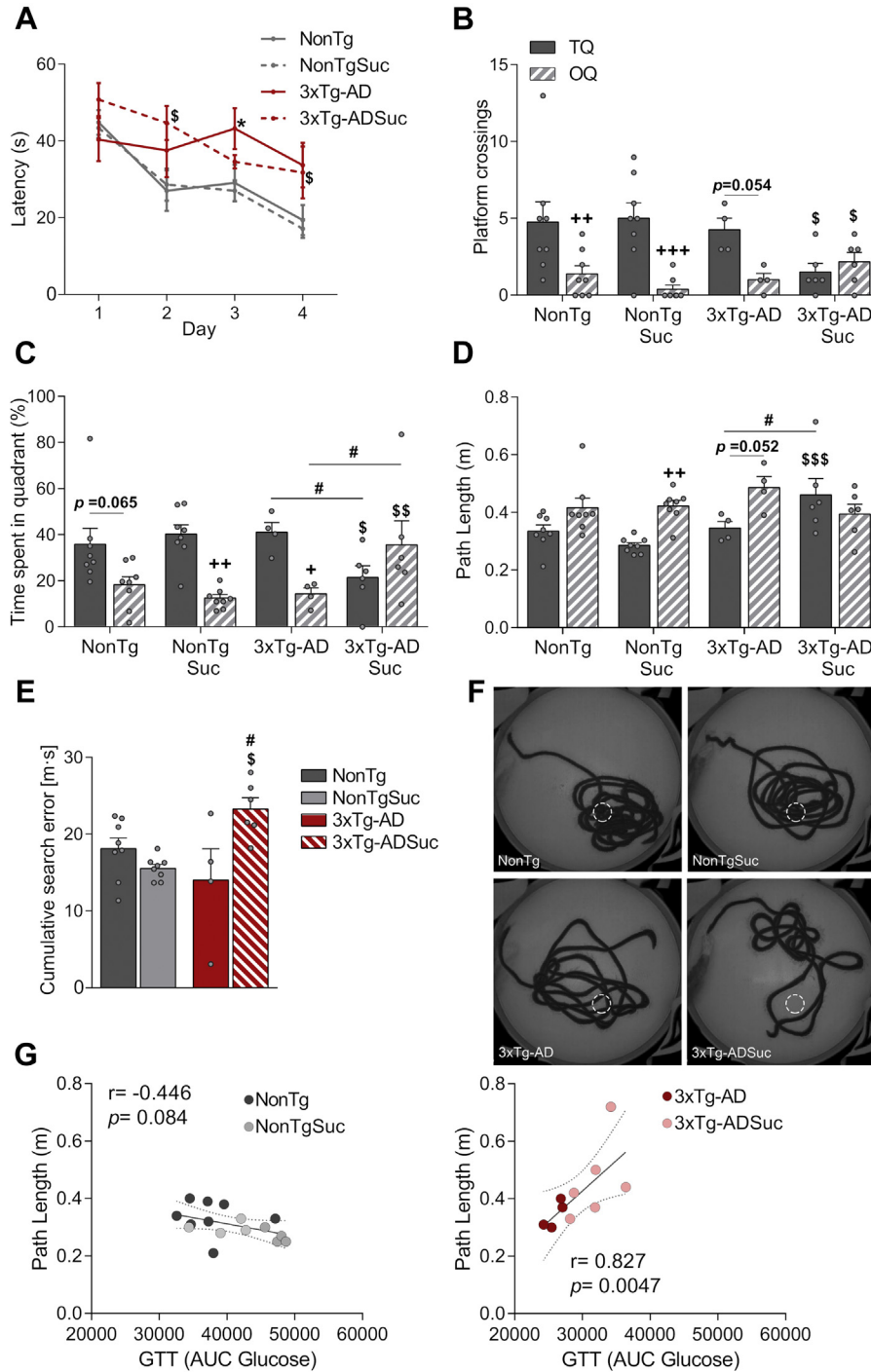
Fig. 1. Learning is impaired in 3xTg-AD mice and memory is compromised in hyperglycemic 3xTg-AD mice. (A) Time spent to reach the platform during the 4 days of learning trials (latency). Untreated and sucrose-treated NonTg mice display a progressive reduction in latencies indicating learning of the task. Latency times are higher in untreated and sucrose-treated 3xTg-mice. The number of platform crossings (B), time spent to reach the platform (C), the average distance to reach the platform (D), and cumulative search error (E) during the probe test show that untreated 3xTg-AD mice, at this age, still retain the capacity to memorize the platform position and that sucrose-treated 3xTg-AD mice search for the platform randomly suggesting no memory retention of its position, which demonstrates a deleterious effect on the memory of 3xTg-AD mice. (F) Representative projections of the path followed by the mice during the probe test. (G) Correlations between the path length and area under the 2-hour blood glucose response curve (AUC; during the oral glucose tolerance test, GTT) in NonTg (left) and 3xTg-AD mice (right). The strong correlation between increasing glucose intolerance and path length found in 3xTg-AD animals further supports that hyperglycemia is strongly related to memory deficits in 3xTg-AD mice. Data are expressed as mean (±SEM) for 4-8 mice per group (points are individual values); $^{+}p < 0.05$, $^{++}p < 0.01$, $^{+++}p < 0.001$ target (TQ) versus opposite quadrant (OQ); $^{*}p < 0.05$ versus NonTg; $^{\$}p < 0.05$, $^{\$\$}p < 0.01$, $^{\$\$\$}p < 0.001$ versus NonTgSuc; $^{\#}p < 0.05$ versus 3xTg-AD. Details of statistical tests and main factor effects are given in Supplementary Table 2. Abbreviations: 3xTg-AD, triple transgenic mouse model of Alzheimer's disease; AUC, area under the curve; NonTg, non-transgenic; SEM, standard error of the mean; Suc, sucrose.

3xTg-AD mice, independently of sucrose treatment, which only exerted a specific decrease in total dendritic length and volume (Supplementary Fig. 4).

The transcriptional activator β-catenin is a key effector molecule of the Wnt signaling pathway, which modulates neuronal differentiation and is altered in AD (Bayod et al., 2015; He and Shen,
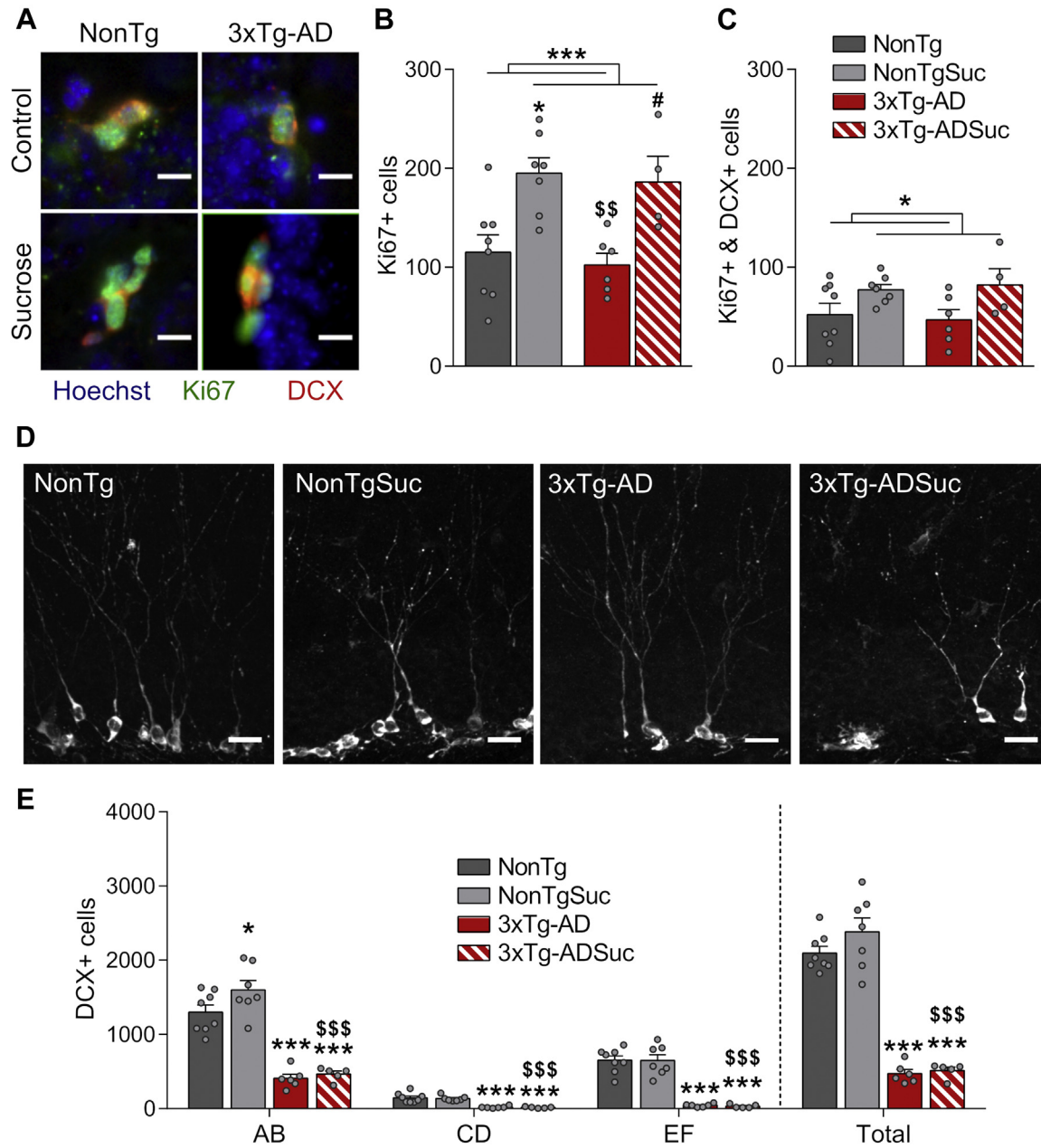
Fig. 2. Hyperglycemia promotes cell proliferation and the number of neuroblasts, while immature neurons are decreased in both control and hyperglycemic 3xTg-AD mice. (A) Confocal microscope images showing Ki67 and doublecortin (DCX) positive cells in the subgranular zone of the hippocampal dentate gyrus. Scale bar, 10 μm. (B) Quantification of Ki67+ cells and (C) quantification of Ki67+ and DCX+ cells. Sucrose treatment promotes cell proliferation, both in general (B) and in DCX cells (C). (D) Confocal microscope images showing DCX positive cells in the hippocampal dentate gyrus. Scale bar, 20 μm. (E) Quantification of the 3 DCX+ cell types: neuroblasts (AB-DCX cells), differentiating neuroblasts (CD-DCX cells), and immature neurons (EF-DCX cells). The number of neuroblasts (AB DCX+ cells) is increased in NonTg mice exposed to sucrose treatment, while the 3 different types of DCX+ cells are reduced in 3xTg-AD mice. Data are expressed as mean (±SEM) for 4-8 mice per group (points indicate individual values); $^*p < 0.05$, $^{***}p < 0.001$ versus NonTg; $^{\$\$}p < 0.01$, $^{\$\$\$}p < 0.001$ versus NonTgSuc; $^\#p < 0.05$ versus 3xTg-AD. Details of statistical tests and main factor effects are given in Supplementary Table 3. Abbreviations: 3xTg-AD, triple transgenic mouse model of Alzheimer's disease; NonTg, non-transgenic; SEM, standard error of the mean; Suc, sucrose.

2009; Varela-Nallar and Inestrosa, 2013; Yu and Malenka, 2003). In an attempt to uncover the defective molecular pathway responsible for the decreased complexity of newly generated neurons in hyperglycemic 3xTg-AD mice, we analyzed the levels of β-catenin in the nucleus and cytoplasm of neuroblasts and both immature and mature neurons (Fig. 4). β-Catenin levels were significantly increased in the nucleus and cytoplasm of neuroblasts of 3xTg-mice, when compared to NonTg mice (Fig. 4B). Hyperglycemia abolished the increase in β-catenin levels in the nucleus of 3xTg-AD

neuroblasts, while increasing its levels in the cytoplasm of NonTg neuroblasts. Nuclear levels of β-catenin were also increased in immature neurons of 3xTg-AD mice (Fig. 3D). Again, hyperglycemia had a negative effect on β-catenin levels in immature neurons from 3xTg-AD mice, since it decreased nuclear and cytoplasm β-catenin levels, when compared to untreated mice. Finally, the absence of sucrose-related alterations in mature neurons (Fig. 4B) further demonstrates the specific effect of disrupted glucose metabolism on immature neurons from 3xTg-AD mice. Thus, our data suggest
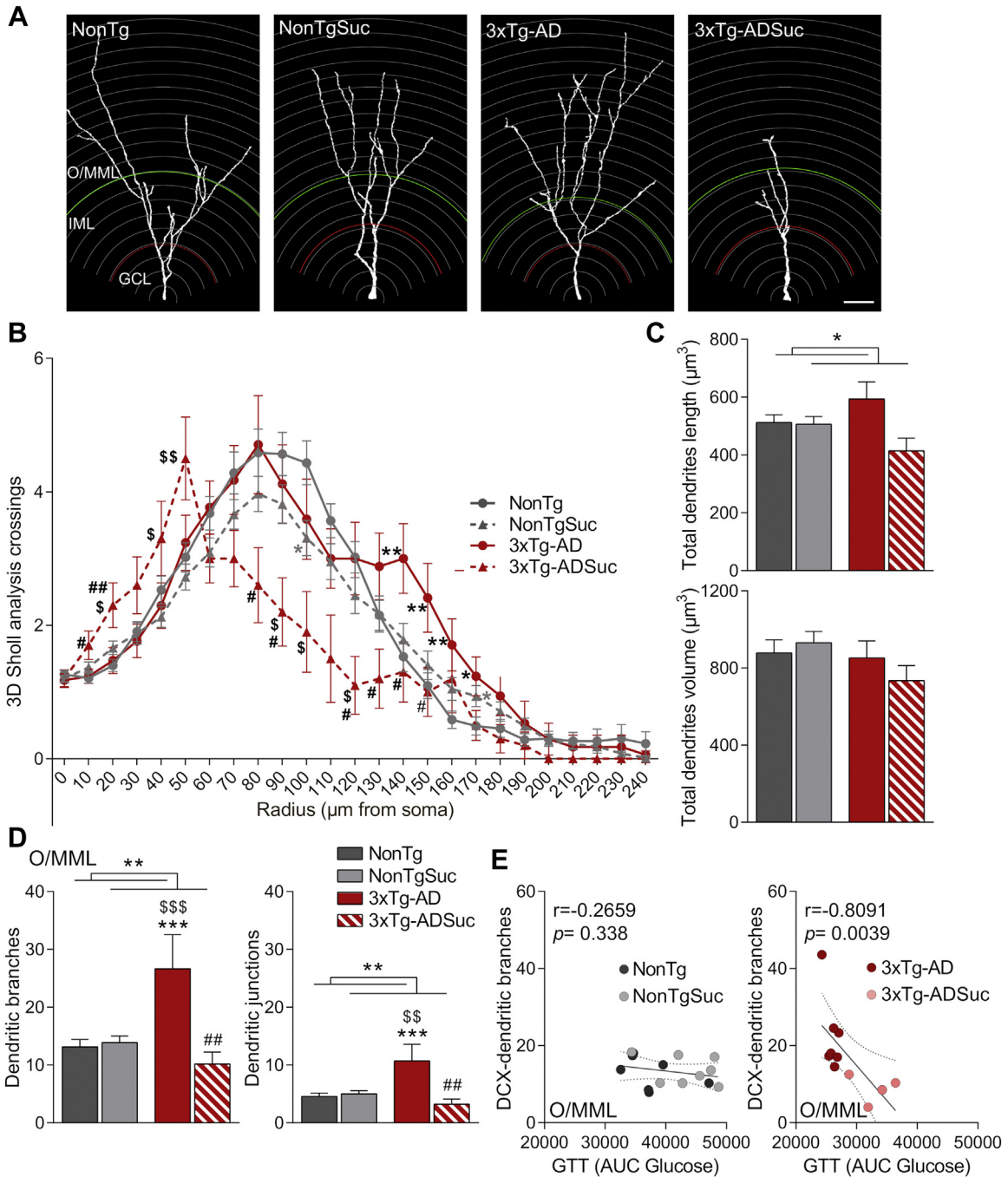
Fig. 3. Loss of dendritic arborization in immature neurons reaching the outer molecular layer in hyperglycemic 3xTg-AD mice. (A) Three-dimensional reconstructions of representative immature neurons reaching the outer and medial molecular layer (O/MML). Red line represents the separation between the GCL and the inner molecular layer (IML) and the green line represents the separation between IML and O/MML. Scale bar, 20 μm. (B) 3D Sholl analysis shows an increased number of dendritic intersections with Sholl spheres in radius 10−50 and a decreased number of dendritic intersections in radius 80−150 in sucrose-treated 3xTg-AD mice when compared to untreated and sucrose-treated NonTg mice. Untreated 3xTg-AD mice display increased dendritic intersections with Sholl spheres in radius 140−170, when compared to untreated NonTg mice, which reflects increased arborization in the O/MML. In radius 100, hyperglycemic NonTg mice show decreased dendritic intersections, when compared to NonTg mice. (C) No significant alterations were observed in the total length and volume of dendrites in untreated and sucrose-treated NonTg or 3xTg-AD mice. (D) Number of dendritic branches (left) and dendritic junctions (right) in the O/MML. In accordance with the Sholl analysis, sucrose-treated 3xTg-mice have decreased the number of dendritic branches and junctions in the O/MML, when compared to untreated 3xTg-AD mice. 3xTg-AD mice display an increased number of dendritic branches and branch junctions in this area when compared to sucrose-treated and untreated NonTg mice. (E) Correlation between the number of dendritic branches in the O/MML and area under the 2-hour blood glucose response curve (AUC; during the oral glucose tolerance test, GTT) in NonTg (left) and 3xTg-AD mice (right) (points indicate individual mouse average value). A strong correlation between increasing glucose intolerance and the number of dendritic branches in the O/MML is found in 3xTg-AD animals, showing that impairment in the dendritic complexity of immature neurons is strongly related to hyperglycemia in 3xTg-AD mice. Data are expressed as mean (±SEM) for 10−65 cells (53/65 or 17/10 cells from 8/8 or 7/4 untreated/sucrose-treated NonTg or 3xTg-AD mice, respectively); $^{*}p < 0.05$, $^{**}p < 0.01$, $^{***}p < 0.001$ versus NonTg; $^{\$}p < 0.05$, $^{\$\$}p < 0.01$, $^{\$\$\$}p < 0.001$ versus NonTgSuc; $^{\#}p < 0.05$, $^{\#\#}p < 0.01$ versus 3xTg-AD. Details of statistical tests and main factor effects are given in Supplementary Table 4. Abbreviations: 3xTg-AD, triple transgenic mouse model of Alzheimer's disease; 3D, three-dimensional; AUC, area under the curve; NonTg, non-transgenic; SEM, standard error of the mean. (For interpretation of the references to color in this figure legend, the reader is referred to the Web version of this article.)
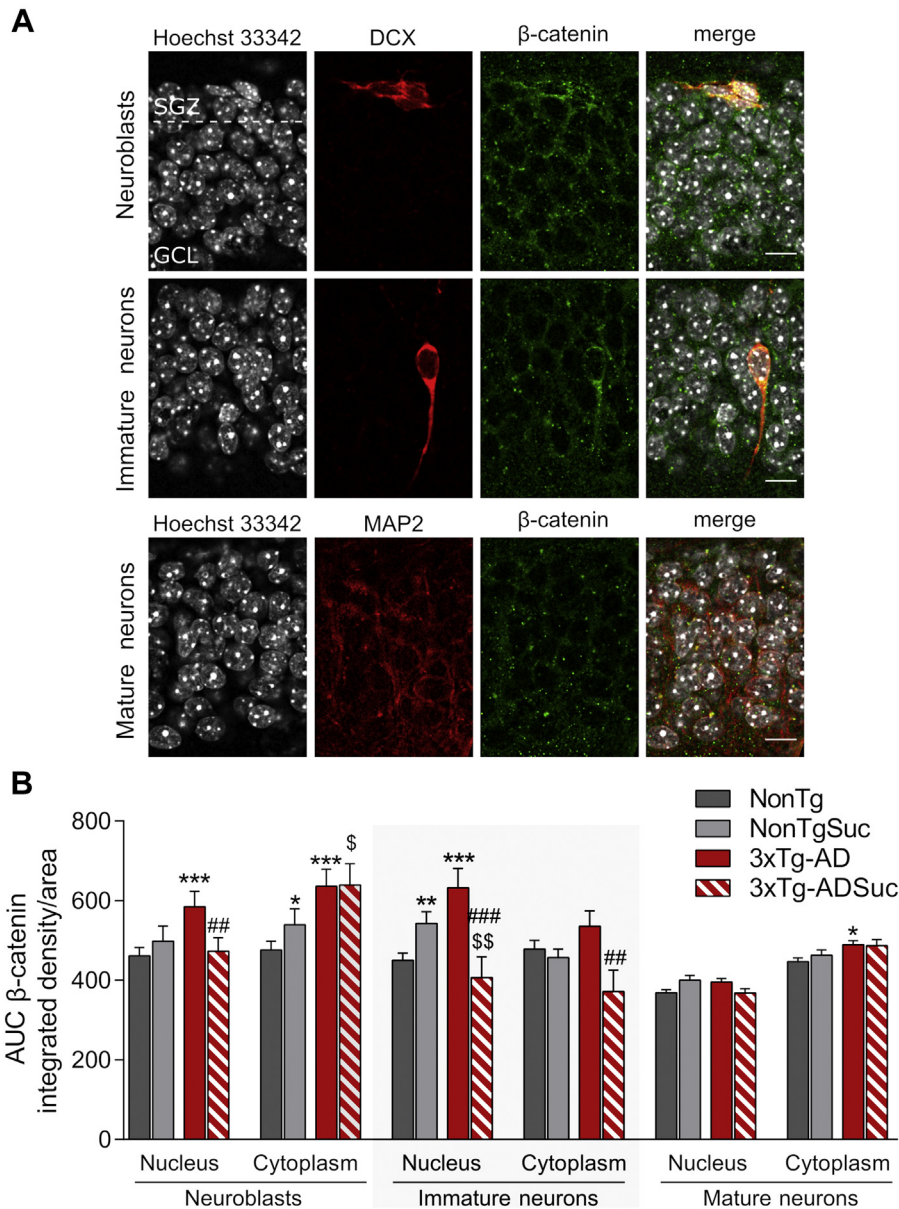
Fig. 4. Chronic hyperglycemia reduces β-catenin levels in the nucleus and cytoplasm of immature 3xTg-AD neurons. (A) Confocal microscope image showing β-catenin positive (in green) and doublecortin (DCX)-positive or microtubule-associated protein 2 staining (in red) in the hippocampal dentate gyrus (nuclei stained with Hoechst 33342). Scale bar, 10 μm. (B) Area under the curve (AUC) of single cell β-catenin integrated density per area (from threshold 1–5) in the nucleus and cytosol of neuroblasts, immature and mature neurons from the dentate gyrus of 8-month-old untreated and sucrose treated NonTg/3xTg-AD mice. A significant and cell-specific reduction in β-catenin levels is found in both the nucleus and cytoplasm of immature neurons from hyperglycemic 3xTg-AD mice when compared to the respective control. In contrast, an increase in these levels is found in immature neurons nucleus from control 3xTg-AD mice, when compared to untreated NonTg mice. Data are expressed as mean (±SEM) for 54/60 to 89/81 cells in untreated and sucrose-treated 3xTg-AD or NonTg neuroblasts, respectively; 31/22 to 98/117 cells in untreated and sucrose-treated 3xTg-AD or NonTg immature neurons, respectively; and 256 cells per group for mature neurons; $^{*}p < 0.01$, $^{**}p < 0.01$, $^{***}p < 0.001$ versus NonTg; $^{\$}p < 0.05$, $^{\$\$}p < 0.01$ versus NonTgSuc; $^{\#\#}p < 0.01$, $^{\#\#\#}p < 0.001$ versus 3xTg-AD. Details of statistical tests and main factor effects are given in Supplementary Table 5. Abbreviations: 3xTg-AD, triple transgenic mouse model of Alzheimer's disease; NonTg, non-transgenic; SEM, standard error of the mean. (For interpretation of the references to color in this figure legend, the reader is referred to the Web version of this article.)

an impairment in the Wnt/β-catenin pathway as a mechanism behind the detrimental effects of hyperglycemia on the dendritic maturation of newborn hippocampal neurons in 3xTg-AD mice.

3.3. Chronic hyperglycemia reduces O/MML dendritic synaptic puncta in immature 3xTg-AD neurons

To further evaluate the potential of newborn neurons to integrate into hippocampal circuitry, putative synaptic contacts were estimated by quantifying the number of PSD95 puncta in the dendrites of immature neurons located in DG IML and O/MML (Fig. 5). Differences were exclusively observed in the O/MML; untreated 3xTg-AD showed a 2.5-fold increase in the total number of synaptic puncta of immature neurons when compared to controlled NonTg mice. This was not due to an increase in the density of puncta (Fig. 5Cv) but to a specific increase in the length of the dendrites occupying this region (Fig. 5Civ). Importantly, in hyperglycemic 3xTg-AD mice, and in agreement with the decreased complexity of immature neuron dendrites in the O/MML (Fig. 3), a significant reduction in the total number of PSD95 puncta was observed when compared to age-
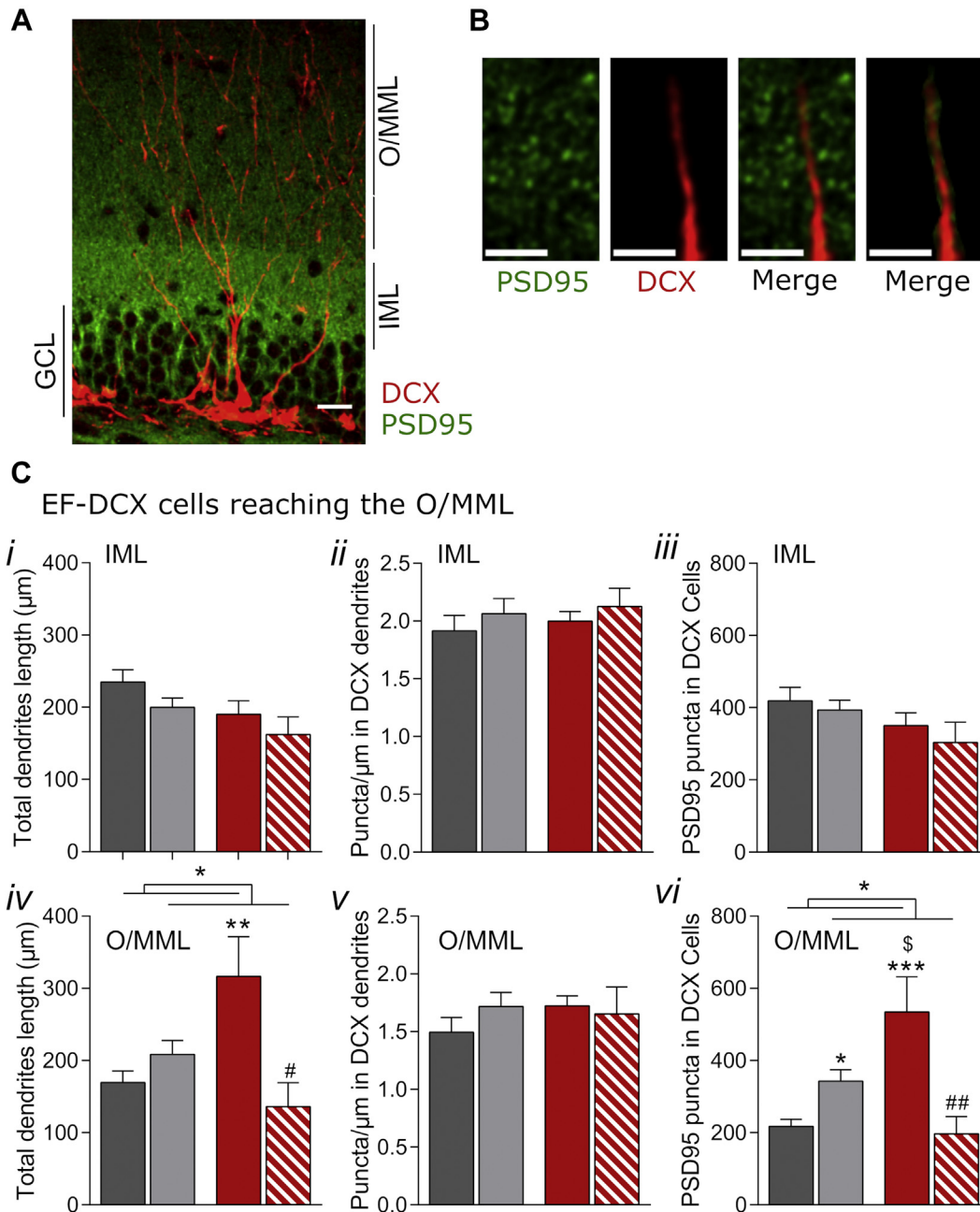
Fig. 5. 3xTg-AD mice show increased total number of dendritic PSD95 puncta in immature neurons reaching the O/MML, which is impaired by chronic hyperglycemia. (A) Confocal microscope image showing post-synaptic density-95 (PSD95) positive and doublecortin (DCX)-positive staining in the hippocampal dentate gyrus. Scale bar, 20 μm (granular cell layer, GCL; inner molecular layer, IML; outer/medial molecular layer, O/MML). (B) Confocal microscope image showing PSD95-positive synaptic puncta colocalizing with a doublecortin (DCX)-positive dendrite. Scale bar, 2 μm. (C) Total dendritic length, number of puncta per DCX dendrite length, and number of PSD95 puncta per cell in the IML (*i*, *ii*, *iii*, respectively) and O/MML (*iv*, *v*, *vi*, respectively). IML total dendrites length (C*i*), number of puncta per DCX dendrite length (C*ii*), and number of PSD95-positive puncta (C*iii*) of immature neurons are unaffected by either treatment or genotype. Importantly, hyperglycemic treatment reduces both total dendrite length (C*iv*) and the number of PSD95 puncta (C*vi*) in DCX cells in the O/MML of 3xTg-AD mice, when compared to untreated mice. Moreover, in the O/MML, untreated 3xTg-AD mice showed an increase in dendritic length and number of PSD95 puncta in dendrites of immature neurons (C*iv* and C*vi*), when compared to untreated NonTg mice. Data are expressed as mean (±SEM) for 53/65 or 17/10 cells from 8/8 or 7/4 untreated/sucrose-treated NonTg or 3xTg-AD mice, respectively; $^{*}p < 0.05$, $^{**}p < 0.01$, $^{***}p < 0.001$ versus NonTg; $^{\$}p < 0.05$ versus NonTgSuc; $^{\#}p < 0.05$, $^{\#\#}p < 0.01$ versus 3xTg-AD. Details of statistical tests and main factor effects are given in Supplementary Table 6. Abbreviations: 3xTg-AD, triple transgenic mouse model of Alzheimer's disease; NonTg, non-transgenic; SEM, standard error of the mean.

matched controls (Fig. 5C*vi*). Globally, the DG of 3xTg-AD mice showed a decrease in the total number of PSD95 puncta in the IML and O/MML (Supplementary Fig. 5) that was associated with a decrease in IML and O/MML volumes (Supplementary Fig. 6). These data suggest that, in 3xTg-AD mice, the increase in the number of O/MML synaptic puncta occurs specifically in immature neurons. Altogether, our data indicate that, in 3xTg-AD mice, hyperglycemia has a negative impact on the maturation of newly generated neurons, reducing their probability of establishing contacts, at the O/MML, with perforant path fibers coming from the EC.

3.4. Chronic hyperglycemia affects long-term synaptic plasticity in the DG of 3xTg-AD mice

The integration of newly generated neurons into hippocampal circuits plays a key role in both synaptic transmission and long-term synaptic plasticity in the DG, which in turn may be involved in the formation of new memories (Massa et al., 2011). Since chronic hyperglycemia affects the maturity of the dendrites of newly generated neurons in 3xTg-AD mice, we hypothesized that synaptic plasticity at the LPP-DG synapses could also be affected. To tackle this hypothesis, we recorded fEPSPs to assess LTP, by stimulating the LPP and recording the evoked potentials in the DG O/MML (Fig. 6A). Experiments were performed in the absence of GABA antagonists considering that young granule

neurons are less inhibited than mature neurons, and thus more sensitive to LTP induction in the presence of GABAergic signal (Saxe et al., 2006). As expected for old animals (Froc et al., 2003), we did not observe any significant LTP in the DG after the application of HFS to the LPP, in conditions of intact inhibition (Fig. 6B–D). However, a nonsignificant trend for late synaptic facilitation was found in recordings from 8-month-old untreated 3xTg-AD mice, when compared to NonTg mice (Fig. 6D). Conversely, a tendency for depression of synaptic transmission upon HFS was found in recordings from hyperglycemic 3xTg-AD mice. Interestingly, the combination of these 2 opposite trends translated into a significant decrease in the synaptic efficacy in the DG of sucrose treated 3xTg-AD mice (Fig. 6D). Strikingly, in 3xTg-AD mice there was a significant correlation between changes in
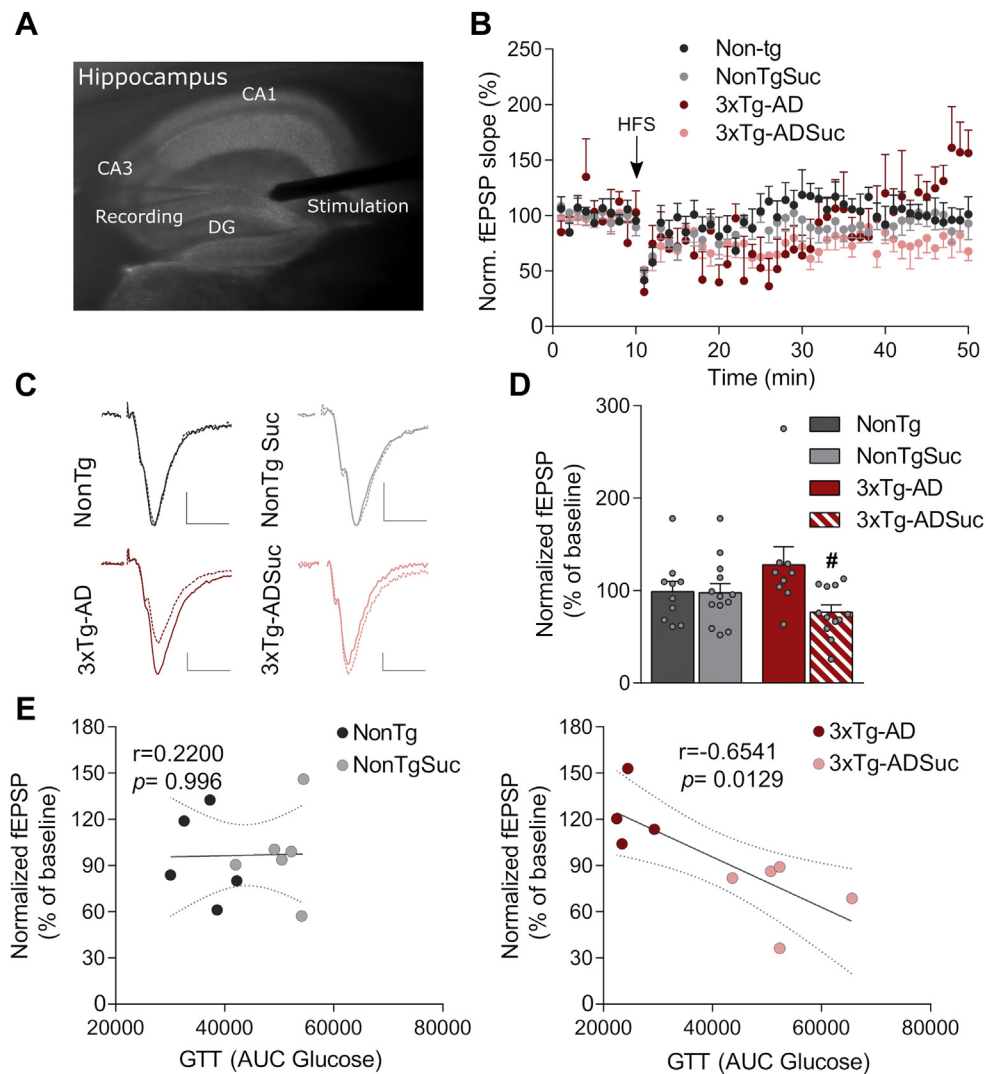

Fig. 6. Long-term synaptic plasticity in the DG is affected in hyperglycemic 3xTg-AD mice. (A) Placement of the stimulation and recording electrodes in the DG for recording field EPSPs (fEPSPs) from LPP synapses. (B) Time course of LTP experiments showing the normalized initial fEPSP slope over time. Following a 10-minute baseline recording with stimulation every 20 s, an HFS protocol (arrow; 1 second, 100 Hz trains of stimulation, repeated 4 times with a 15 seconds interval) was used to attempt to induce long-term potentiation at LPP synapses onto DG granule cells. Data are expressed as mean (±SEM) for 9–14 slices per group. (C) Sample averaged fEPSPs for each experimental condition. Dotted line, baseline; solid line, 30–40 minutes after HFS. Scale: 0.1 mV × 4 ms. (D) Summary graph of changes in synaptic efficacy at 30–40 minutes after HFS. As expected for older mice in the presence of intact inhibitory synaptic transmission, no change in synaptic efficacy was observed for any of the experimental groups, except for the hyperglycemic 3xTg-AD that showed a trend for depression of synaptic transmission compared to untreated 3xTg-AD mice. Data are expressed as mean (±SEM) for 9–14 slices per group (points indicate individual values); #$p < 0.05$ versus 3xTg-AD. (E) Correlations between normalized fEPSP values (averaged values/animals) and area under the 2-hour blood glucose response curve (AUC; during the oral glucose tolerance test, GTT) in NonTg (left) and 3xTg-AD mice (right). A strong correlation between increasing glucose intolerance and normalized fEPSP is found in 3xTg-AD animals, showing that changes in synaptic efficacy are associated with hyperglycemia in 3xTg-AD mice. Details of statistical tests and main factor effects are given in Supplementary Table 7. Abbreviations: 3xTg-AD, triple transgenic mouse model of Alzheimer's disease; AUC, area under the curve; DE, dentate gyrus; EPSP, excitatory postsynaptic potential; HFS, high-frequency stimulation; LTP, long-term potentiation; NonTg, non-transgenic; SEM, standard error of the mean.

synaptic efficacy and blood glucose levels that was not observed in NonTg mice (Fig. 6E). This further demonstrates that chronic hyperglycemia significantly impacts synaptic plasticity at LPP-DG synapses in the context of an AD-like challenge, which may be attributed to the reduced complexity of newly generated neurons in the DG O/MML.

3.5. Multivariate analysis of hyperglycemia, behavior, and neurogenesis data

We have shown different analyses indicating that blood glucose levels (GTT) correlate with behavioral parameters (Fig. 1G), the morphology of newborn cells (Fig. 3E), and the electrophysiological activity in the DG (Fig. 6E). To better explore possible associations between different variables, we have also performed a correlation matrix analysis. Our data revealed that GTT significantly correlated with behavioral parameters and the number of newborn neurons at different maturational stages. Additionally, we observed significant correlations between several neurogenesis and behavior features (Supplementary Fig. 7). However, data from transgenic mice clustered together and may act as outliers, which may induce some inflation of our correlation coefficients and lead to the detection of spurious correlations (Makin and De Xivry, 2019). Therefore, although we performed correlational analysis using the Spearman's rank test, which is not much affected by outliers (de Winter et al., 2016), we decided to analyze data from NonTg (Supplementary Fig. 8) and 3xTg-AD (Supplementary Fig. 9) mice separately. In NonTg mice, glucose tolerance (GTT) negatively correlated with one spatial negative memory parameter, the path length in the target quadrant until reaching the platform, making it difficult to infer whether memory scores associate with hyperglycemia. However, in 3xTg-AD mice, GTT correlated with several behavioral parameters, suggesting that glucose intolerance associated with poor memory. 3xTg-AD GTT also correlated with 2 parameters related to the morphology of newborn neurons (the number of dendritic branches and junctions in the OMML). Curiously, in both NonTg and 3xTg-AD mice, the number of proliferating cells correlated with several behavioral parameters, although in opposite directions (Supplementary Figs. 8 and 9). Thus, in general terms, in NonTg mice, the number of proliferating cells (Ki67+ cells) associated with better memory performance, while in 3xTg-AD mice it associated with worse MWM scores. Interestingly, in 3xTg-AD mice, CSE (an index of erratic search strategies) correlated negatively with the number of young newborn neurons (EF cells) and the volume of their dendrites (Supplementary Fig. 9). In summary, these analyses suggest that hyperglycemia, neurogenesis, and memory scores are consistently associated.

Our results indicate that hyperglycemia exerts a negative effect specifically on 3xTg-AD mice, affecting behavior and neurogenesis-related parameters. We have performed an in-depth analysis of our data using PCA to further evaluate the differences induced by hyperglycemia. In our PCA, the first 6 principal components explained 78.90% of the variance of our data (PC1: 23.09%, PC2 20.19%, PC3 13.38%, PC4 9.00%, PC5 7.17%, and PC6 6.07%). Importantly, using only components 1 and 2 we were able to differentiate 3 nonoverlapping groups: NonTg (independently of their treatment with sucrose), untreated 3xTg-AD mice, and 3xTg-AD mice treated with sucrose (Fig. 7). Thus, PCA corroborated that sucrose treatment exerted a specific effect on 3xTg-AD mice.

Summarizing, our in-depth data analysis corroborated that blood glucose levels affect both neurogenesis and memory function and that hyperglycemia has a specific detrimental effect in 3xTg-AD mice.

4. Discussion

One of the emerging concepts associated with age-related neurocognitive diseases is the multimorbidity that arises from common risk factors and mechanisms, possibly resulting in early disease onset (Figueira et al., 2016). This concept is changing the paradigm used to treat these diseases to a more integrative approach. Moreover, increasing evidence shows that AD and T2D, 2 age-associated chronic diseases, share common features and are intrinsically associated. Here, we demonstrate that chronic hyperglycemia affects the hippocampal neurogenic reserve of 3xTg-AD mice, considered as the capacity of the hippocampus to produce new neurons, which adequately integrate into hippocampal memory circuits. Hyperglycemia reduces the possibility of proper integration of newly generated neurons in the hippocampus of 3xTg-AD mice (reduced dendritic complexity and number of synaptic puncta in the region of contact with the axons projecting from the EC), resulting in subtle alterations in synaptic plasticity and defective spatial memory. We also show that immature neurons in 8-month-old 3xTg-AD mice display an increase in
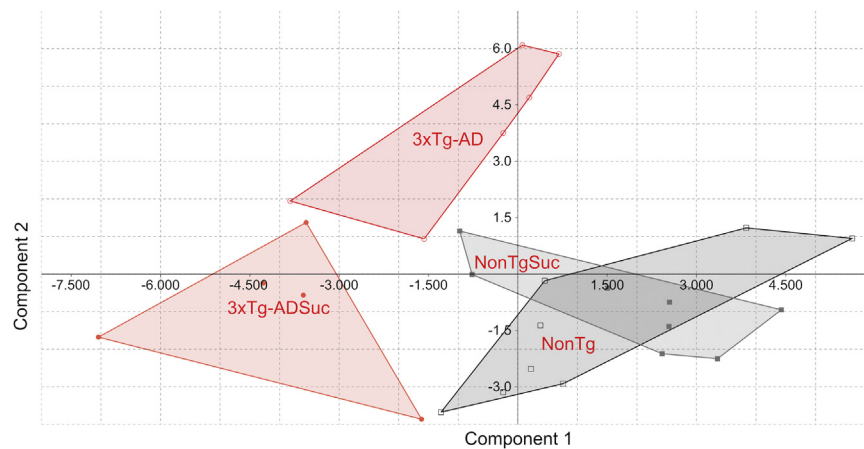

Fig. 7. Principal component analysis reveals differences induced by sucrose treatment specifically in 3xTg-AD mice. PCA scores for each mouse are represented in the graph as dots (squares for NonTg mice, circles for 3xTgAD mice, open dots for mice without sucrose treatment, and filled dots for mice treated with sucrose). Convex hull areas for each group show 3 segregated regions corresponding to NonTg mice (with or without sucrose treatment), 3xTg-AD mice, and sucrose-treated 3xTg-AD mice. Data are available in the supplemental data file "Suppl PCA data.xlsx." Abbreviations: 3xTg-AD, triple transgenic mouse model of Alzheimer's disease; NonTg, non-transgenic; PCA, Principal component analysis.

dendritic arborization and the number of DG O/MML synaptic contacts. These may be interpreted as a compensatory mechanism that allows the animals to maintain a certain degree of adaptation to the cognitive demands. Importantly, this apparent compensatory mechanism is severely compromised by the perturbation in glucose metabolism.

The existence of adult neurogenesis has been described in numerous species, including rodents and primates (Patzke et al., 2015). Adult hippocampal neurogenesis and the production of several hundreds of new neurons per day were previously described in humans (Eriksson et al., 1998; Spalding et al., 2013). Recent studies relaunched the discussion by reporting that neurogenesis does not occur in adulthood (Sorrells et al., 2018), or either persists along with aging (Boldrini et al., 2018). However, a very recent and meticulous work by Moreno-Jiménez et al. (2019) demonstrated that thousands of (DCX+) DG immature neurons can be found in healthy aged human subjects, strongly supporting the existence of adult hippocampal neurogenesis in humans and its persistence into late age. Quite importantly, these authors also reported that the number and maturation of these cells decrease in AD patients with the progression of Braak stages, that is, with the degree of AD pathology (Moreno-Jiménez et al., 2019).

Results concerning adult neurogenesis in AD models may seem contradictory, but differences between studies may be attributed to the use of different disease models, the age of the animals, and the methods used to analyze neurogenesis. Some authors even suggested that adult neurogenesis is enhanced in AD after analyzing proliferation markers. Indeed, increased general cell proliferation was described at different ages (3 and 12 months) in PDGF-APPSw,Ind mice (Jin et al., 2004; López-Toledano and Shelanski, 2007). Furthermore, 9- to 12-month-old Tg9291 mice presented an increased number of proliferating neuronal progenitors (Kolecki et al., 2008), while 3-month-old PDGF-APPSw,Ind mice showed more neuroblasts/young neurons (identified by the expression of the polysialylated-neural cell adhesion molecule PSA-NCAM) when compared to control mice (López-Toledano and Shelanski, 2007). Although these studies reported increased neurogenesis in various AD mouse models, quantification of proliferating cells is not enough for such conclusion as the survival of neuronal progenitors or young neurons should be also evaluated. Importantly, a vast number of studies performed in AD mouse models identified decreased adult neurogenesis as a contributor for AD symptoms (Haughey et al., 2002; Verret et al., 2007; Wang et al., 2004; reviewed in Chuang, 2010; Sung et al., 2020). Herein, we observed normal cell proliferation in 8-month-old 3xTg-AD male mice, both in general and DCX+ cells. However, similar to what was described in Valero et al. (2014) for 6-month-old female 3xTg-AD mice, we detected a decrease in the number of neuroblasts, differentiating neuroblasts and immature neurons. Our data also suggest that the decrease in the number of neurogenic cells is not enough to affect cognitive capacity, in our conditions and at this age (see below), which, we hypothesize, may be related to the capacity of the remaining immature neurons to increase their complexity and establish more contacts with EC projection fibers. Taking into account the data obtained by Moreno-Jiménez et al. (2019) in humans, indicating that the number of DCX+ cells decreases with the development of the disease, it would have been interesting to further analyze the morphology of these cells (i.e., dendrites complexity), and evaluate whether it is related to Braak stages.

The hippocampal neurogenic reserve may be considered as a component of the cognitive reserve (Valero et al., 2016). In AD, the development of a metabolic syndrome such as T2D can be framed as a lifestyle shaping factor that, continuously and over a long period, may strongly affect brain's cognitive reserve, promoting the early appearance of symptoms. Although the cognitive reserve

cannot be measured per se, several parameters have been proposed to reflect the brain's functional potential, namely brain volume, synapse density, neuronal number, and dendritic complexity (Valero et al., 2016). Given that the hippocampus is one of the brain regions affected in AD (Gallagher and Koh, 2011), the evaluation of these parameters may be translated into a reliable measure of the functional status of the brain. Due to both the reduced volume of the DG and the number of synaptic puncta in 8-month-old 3xTg-AD mice, these animals are expected to present a poor cognitive reserve, which would be reflected as a perturbed cognitive function. At first sight, our data suggest that this was not the case since 3xTg-AD mice displayed similar spatial memory scores to their age-matched controls. However, specific characteristics in our experimental design may explain this apparent contradiction and should be taken into account when interpreting the results that: first, our mice were housed with mild environmental enrichment conditions, in the presence of a malleable paper bag that was changed twice a week, and environmental enrichment is known to recover memory function in mouse models of AD (Llorens-Martín, 2018; Polito et al., 2014; Valero et al., 2011; Verret et al., 2013); second, we used a facilitated MWM paradigm to improve the learning of the task (Valero et al., 2014); and finally, 50% of our 3xTg-AD mice did not learn the task and showed thigmotaxia (i.e., constant searching in the walls of the maze associated to anxiety; Treit and Fundytus, 1988), and were excluded from this analysis. Concomitantly, our observations suggest that at least 50% of our aged 3xTg-AD animals retain some level of cognitive reserve that allows them to use alternative strategies to face a cognitive and stressful challenge. However, the cognitive reserve of these 3xTg-AD mice is also tremendously fragile, as the additional challenge of chronic hyperglycemia leads to a total disruption of memory function. We can thus hypothesize that, at this age (8 months), the cognitive reserve threshold of 3xTg-AD mice was not yet reached and that, with further aging and ensuing the reduction of neurogenesis, cognitive deficits will manifest. Importantly, the hippocampal neurogenic niche in 3xTg-AD mice maintained some capacity of producing newborn neurons. Even more, newborn neurons in 3xTg-AD mice showed increased complexity and number of PSD95 puncta in the dendrites that reach the O/MML, where they establish synaptic contacts with the fibers arriving from the EC. This may act as a compensatory effect mediated by the lack of pre-existing mature synaptic contacts. Furthermore, maturing newborn neurons compete with already mature neurons to establish synaptic contacts, and may displace and contribute to the elimination of pre-existing synapses (Toni et al., 2007). Thus, we may speculate that, due to the general decrease in the number of synaptic puncta seen in 3xTg-AD mice, the few newborn neurons that develop enough to reach the O/MML may arborize more profusely because of the reduced competition with pre-existing neurons and the higher availability of potential sites for synaptic contacts. Importantly, our results suggest that hyperglycemia affects this compensatory mechanism. However, further studies will be required to adequately test this hypothesis.

The possible compensatory effects observed in newly generated neurons of 3xTg-AD mice may require the activation of specific molecular pathways that promote the dendritic arborization of immature neurons, such as the Wnt/β-catenin signaling pathway. This pathway has been shown to enhance dendritic complexity in hippocampal neurons (Yu and Malenka, 2003), to be reduced in AD brains (Zhang et al., 1998) and dysfunctional in hippocampal neurons after exposure to Aβ (Krieghoff et al., 2006), potentially affecting neuronal differentiation. However, we observed a specific increase in β-catenin levels in 3xTg-AD mice, both in the nucleus and cytoplasm of hippocampal neurogenic cells, namely DCX-labeled neuroblasts and immature neurons. Such an increase in β-
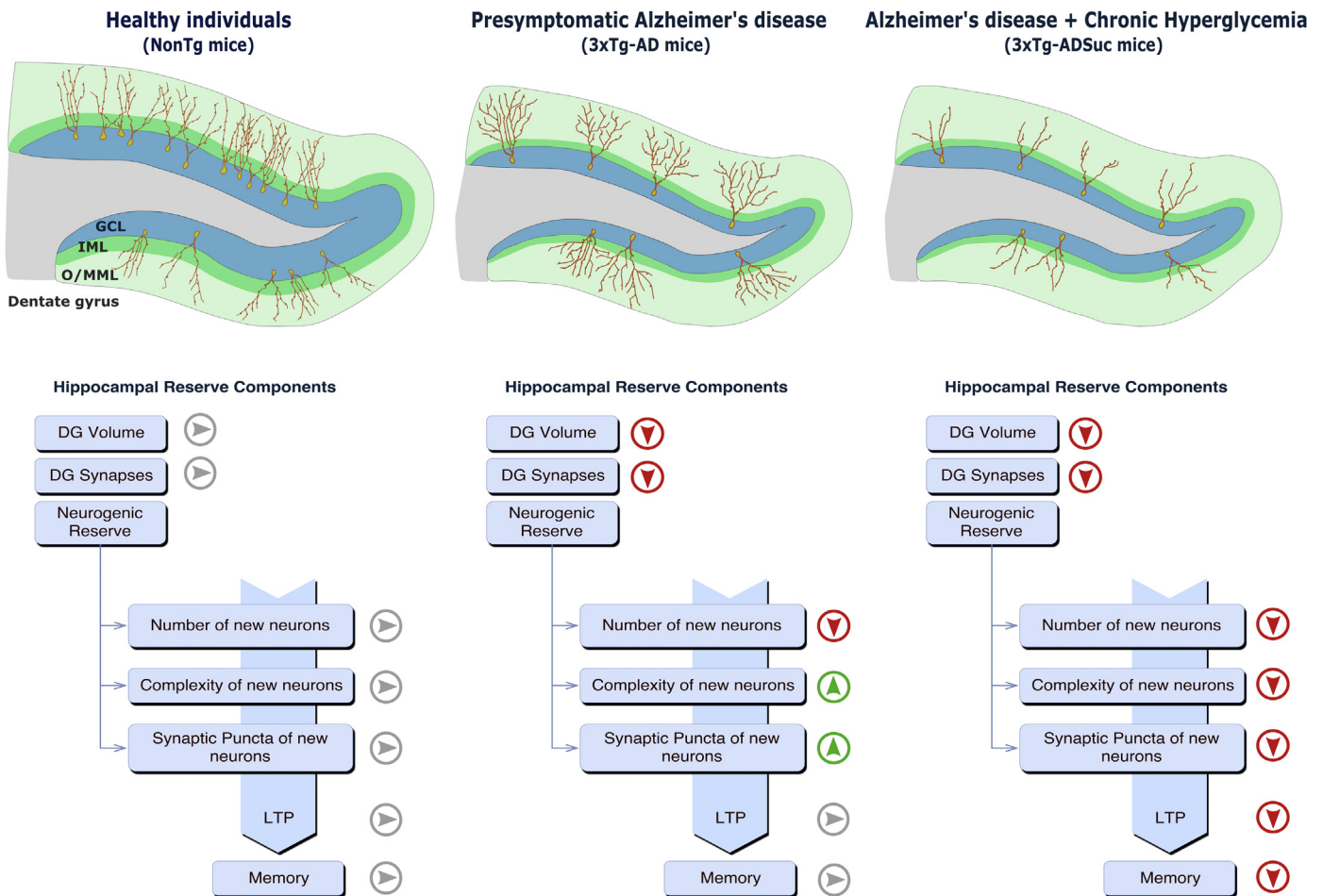
Fig. 8. Schematic representation of the detrimental effect of chronic hyperglycemia and AD-related impairments on the hippocampal neurogenic reserve and memory. Abbreviations: AD, Alzheimer's disease; DG, dentate gyrus; GCL, granular cell layer; IML inner molecular layer; LTP, long-term potentiation; O/MML, outer and medial molecular layer. Hippocampal immature neurons are represented in brown. (For interpretation of the references to color in this figure legend, the reader is referred to the Web version of this article.)

catenin levels may promote the increase in the dendritic complexity observed in 3xTg-AD newborn neurons. β-Catenin is a versatile protein that integrates a myriad of functions in different cellular locations, including the nucleus, cytosol, and cellular membranes (Valenta et al., 2012) and, for this reason, its regulation is dependent on multiple interplaying factors. β-Catenin activity is mainly regulated by constitutive proteasomal degradation, which is promoted through phosphorylation by glycogen synthase kinase-3β (Hur and Zhou, 2010), an enzyme activated in AD (Maqbool et al., 2016). Thus, glycogen synthase kinase-3β activation may increase β-catenin degradation, impairing cellular processes dependent on its normal function. In 3xTg-AD mice, hyperglycemia significantly reduced nuclear and cytoplasmic β-catenin levels in newly generated hippocampal cells, which may account for the decreased maturation and dendritic atrophy found in these cells. Nevertheless, further experiments are required to fully understand the molecular mechanisms behind the changes induced by hyperglycemia in β-catenin levels and their consequences for newly generated neurons in the context of AD. It would be interesting to both overexpress and knockdown beta-catenin in immature neurons to evaluate if these conditions recapitulate the changes in maturation observed in our experiments. This would also allow evaluating the possible therapeutic potential of β-catenin overexpression as a promoter of maturation and functional integration of immature neurons into the hippocampal

neurogenic reserve, thus protecting against the deleterious effects of hyperglycemia in AD.

Following the rationale of the hippocampal neurogenic reserve, hyperglycemic 3xTg-AD mice combine several indicators of reduced cognitive reserve: decreased DG volume, reduced number of synaptic puncta, and low number of newly generated neurons presenting atrophic dendritic complexity. This reduction in neurogenic capacity might express itself through the altered synaptic plasticity observed in response to LPP stimulation in the presence of intact inhibitory synaptic transmission. Altogether, our data indicate that chronic hyperglycemia may further compromise the already deteriorated cognitive reserve in the context of AD, ultimately resulting in the incapacity to respond to cognitive challenge(s), as manifested by the impairment in memory observed in our mouse model of AD (Fig. 8).

5. Conclusion

Overall, we clearly demonstrate that chronic hyperglycemia affects the adult hippocampal neurogenic reserve in the 3xTg-AD transgenic mouse model, inducing defective learning and memory loss, and accelerating AD-like impairments. Disturbance of Wnt/β-catenin signaling by chronic hyperglycemia may be responsible for the deficient morphological maturation of newly generated neurons, contributing to the depletion of the hippocampal neurogenic

reserve and triggering cognitive deficits. Defining the molecular mechanisms that influence the maturation and incorporation of newly generated neurons into memory circuits under conditions of perturbed glucose metabolism will allow the development of therapeutic strategies aimed at promoting the hippocampal adult neurogenic reserve. This may likely shield against age-related neuronal degeneration/loss in a brain region required for processing of learning and memory, thereby delaying AD symptoms.

Disclosure statement

The authors declare no conflicts of interest and no competing financial interests.

CRediT authorship contribution statement

Elisabete Ferreiro: Investigation, Conceptualization, Methodology, Software, Validation, Formal analysis, Supervision, Visualization, Writing - original draft, Writing - review & editing. **Mariagrazia Lanzillo:** Investigation. **Diogo Canhoto:** Investigation. **António M. Carvalho da Silva:** Investigation. **Ildete L. Ferreira:** Investigation. **Giorgia Mastrella:** Investigation. **Paulo Pinheiro:** Investigation, Validation, Formal analysis, Writing - review & editing. **Jorge Valero:** Investigation, Conceptualization, Methodology, Software, Validation, Formal analysis, Visualization, Writing - review & editing. **A. Cristina Rego:** Conceptualization, Supervision, Resources, Project administration, Funding acquisition, Writing - review & editing.

Acknowledgements

Appendix A. Supplementary data

Supplementary data to this article can be found online at https://doi.org/10.1016/j.neurobiolaging.2020.04.003.

References

Bayod, S., Felice, P., Andrés, P., Rosa, P., Camins, A., Pallàs, M., Canudas, A.M., 2015. Downregulation of canonical Wnt signaling in hippocampus of SAMP8 mice. Neurobiol. Aging 36, 720–729.

Boldrini, M., Fulmore, C.A., Tartt, A.N., Simeon, L.R., Pavlova, I., Poposka, V., Rosoklija, G.B., Stankov, A., Arango, V., Dwork, A.J., Hen, R., Mann, J.J., 2018. Human hippocampal neurogenesis persists throughout aging. Cell Stem Cell 22, 589–599.e5.

Bologna-Molina, R., Mosqueda-Taylor, A., Molina-Frechero, N., Mori-Estevez, A.D., Sanchez-Acuna, G., 2013. Comparison of the value of PCNA and Ki-67 as markers of cell proliferation in ameloblastic tumors. Med. Oral. Patol. Oral. Cir. Bucal. 18, e174–e179.

Carvalho, C., Cardoso, S., Correia, S.C., Santos, R.X., Santos, M.S., Baldeiras, I., Oliveira, C.R., Moreira, P.I., 2012. Metabolic alterations induced by sucrose intake and Alzheimer's disease promote similar brain mitochondrial abnormalities. Diabetes 61, 1234–1242.

Casadesus, G., Moreira, P.I., Nunomura, A., Siedlak, S.L., Bligh-Glover, W., Balraj, E., Petot, G., Smith, M.A., Perry, G., 2007. Indices of metabolic dysfunction and oxidative stress. Neurochem. Res. 32, 717–722.

Chuang, T.T., 2010. Neurogenesis in mouse models of Alzheimer's disease. Biochim. Biophys. Acta 1802, 872–880.

Cowie, C.C., Rust, K.F., Ford, E.S., Eberhardt, M.S., Byrd-Holt, D.D., Li, C., Williams, D.E., Gregg, E.W., Bainbridge, K.E., Saydah, S.H., Geiss, L.S., 2009. Full accounting of diabetes and pre-diabetes in the U.S. population in 1988-1994 and 2005-2006. Diabetes Care 32, 287–294.

de la Monte, S.M., 2012. Brain insulin resistance and deficiency as therapeutic targets in Alzheimer's disease. Curr. Alzheimer Res. 9, 35–66.

de Winter, J.C.F., Gosling, S.D., Potter, J., 2016. Comparing the Pearson and Spearman correlation coefficients across distributions and sample sizes: a tutorial using simulations and empirical data. Psychol. Methods 21, 273–290.

Dumitriu, D., Berger, S.I., Hamo, C., Hara, Y., Bailey, M., Hamo, A., Grossman, Y.S., Janssen, W.G., Morrison, J.H., 2012. Vamping: stereology-based automated quantification of fluorescent puncta size and density. J. Neurosci. Methods 209, 97–105.

Encinas, J.M., Michurina, T.V., Peunova, N., Park, J.H., Tordo, J., Peterson, D.A., Fishell, G., Koulakov, A., Enikolopov, G., 2011. Division-coupled astrocytic differentiation and age-related depletion of neural stem cells in the adult hippocampus. Cell Stem Cell 8, 566–579.

Eriksson, P.S., Perfilieva, E., Bjork-Eriksson, T., Alborn, A.M., Nordborg, C., Peterson, D.A., Gage, F.H., 1998. Neurogenesis in the adult human hippocampus. Nat. Med. 4, 1313–1317.

Ferreira, I.L., Resende, R., Ferreiro, E., Rego, A.C., Pereira, C.F., 2010. Multiple defects in energy metabolism in Alzheimer's disease. Curr. Drug Targets 11, 1193–1206.

Figueira, I., Fernandes, A., Mladenovic Djordjevic, A., Lopez-Contreras, A., Henriques, C.M., Selman, C., Ferreiro, E., Gonos, E.S., Trejo, J.L., Misra, J., Rasmussen, L.J., Xapelli, S., Ellam, T., Bellantuono, I., 2016. Interventions for age-related diseases: shifting the paradigm. Mech. Ageing Dev. 160, 69–92.

Froc, D.J., Eadie, B., Li, A.M., Wodtke, K., Tse, M., Christie, B.R., 2003. Reduced synaptic plasticity in the lateral perforant path input to the dentate gyrus of aged C57BL/6 mice. J. Neurophysiol. 90, 32–38.

Gallagher, M., Koh, M.T., 2011. Episodic memory on the path to Alzheimer's disease. Curr. Opin. Neurobiol. 21, 929–934.

Gao, X., Arlotta, P., Macklis, J.D., Chen, J., 2007. Conditional knock-out of beta-catenin in postnatal-born dentate gyrus granule neurons results in dendritic malformation. J. Neurosci. 27, 14317–14325.

Garthe, A., Kempermann, G., 2013. An old test for new neurons: refining the Morris water maze to study the functional relevance of adult hippocampal neurogenesis. Front Neurosci. 7, 63.

Haughey, N.J., Nath, A., Chan, S.L., Borchard, A.C., Rao, M.S., Mattson, M.P., 2002. Disruption of neurogenesis by amyloid β-peptide, and perturbed neural progenitor cell homeostasis, in models of Alzheimer's disease. J. Neurochem. 83, 1509–1524.

He, P., Shen, Y., 2009. Interruption of β-catenin signaling reduces neurogenesis in Alzheimer's disease. J. Neurosci. 29, 6545–6557.

Herbert, A.D., Carr, A.M., Hoffmann, E., 2014. FindFoci: a focus detection algorithm with automated parameter training that closely matches human assignments, reduces human inconsistencies and increases speed of analysis. PLoS One 9, e114749.

Hur, E.M., Zhou, F.Q., 2010. GSK3 signalling in neural development. Nat. Rev. Neurosci. 11, 539–551.

Ilin, A., Raiko, T., 2010. Practical approaches to principal component analysis in the presence of missing values. J. Mach. Learn. Res. 11, 1957–2000.

Jin, K., Galvan, V., Xie, L., Mao, X.O., Gorostiza, O.F., Bredesen, D.E., Greenberg, D.A., 2004. Enhanced neurogenesis in Alzheimer's disease transgenic (PDGF-APP Sw,Ind) mice. Proc. Natl. Acad. Sci. U. S. A. 101, 13363–13367.

Kempermann, G., 2008. The neurogenic reserve hypothesis: what is adult hippocampal neurogenesis good for? Trends Neurosci. 31, 163–169.

Kempermann, G., Jessberger, S., Steiner, B., Kronenberg, G., 2004. Milestones of neuronal development in the adult hippocampus. Trends Neurosci. 27, 447–452.

Kolecki, R., LaFauci, G., Rubenstein, R., Mazur-Kolecka, B., Kaczmarski, W., Frackowiak, J., 2008. The effect of amyloidosis-β and ageing on proliferation of neuronal progenitor cells in APP-transgenic mouse hippocampus and in culture. Acta Neuropathol 116, 419–424.

Krieghoff, E., Behrens, J., Mayr, B., 2006. Nucleo-cytoplasmic distribution of beta-catenin is regulated by retention. J. Cell Sci 119, 1453–1463.

Kroner, Z., 2009. The relationship between Alzheimer's disease and diabetes: type 3 diabetes? Altern. Med. Rev. 14, 373–379.

Lie, D.C., Colamarino, S.A., Song, H.J., Desire, L., Mira, H., Consiglio, A., Lein, E.S., Jessberger, S., Lansford, H., Dearie, A.R., Gage, F.H., 2005. Wnt signalling regulates adult hippocampal neurogenesis. Nature 437, 1370–1375.

Llorens-Martín, M., 2018. Exercising new neurons to vanquish Alzheimer disease. Brain Plast. 4, 111–126.

Longair, M.H., Baker, D.A., Armstrong, J.D., 2011. Simple Neurite Tracer: open source software for reconstruction, visualization and analysis of neuronal processes. Bioinformatics 27, 2453—2454.

López-Toledano, M.A., Shelanski, M.L., 2007. Increased neurogenesis in young transgenic mice overexpressing human APPSw,Ind. J. Alzheimers Dis. 12, 229—240.

Makin, T.R., De Xivry, J.J.O., 2019. Ten common statistical mistakes to watch out for when writing or reviewing a manuscript. Elife 8, pii: e48173.

Maqbool, M., Mobashir, M., Hoda, N., 2016. Pivotal role of glycogen synthase kinase-3: a therapeutic target for Alzheimer's disease. Eur. J. Med. Chem. 107, 63—81.

Massa, F., Koehl, M., Wiesner, T., Grosjean, N., Revest, J.M., Piazza, P.V., Abrous, D.N., Oliet, S.H., 2011. Conditional reduction of adult neurogenesis impairs bidirectional hippocampal synaptic plasticity. Proc. Natl. Acad. Sci. U S A. 108, 6644—6649.

Matos, C.A., Nóbrega, C., Louros, S.R., Almeida, B., Ferreiro, E., Valero, J., De Almeida, L.P., Macedo-Ribeiro, S., Carvalho, A.L., 2016. Ataxin-3 phosphorylation decreases neuronal defects in spinocerebellar ataxia type 3 models. J. Cell Biol. 212, 465—480.

Moreno-Jiménez, E.P., Flor-García, M., Terreros-Roncal, J., Rábano, A., Cafini, F., Pallas-Bazarra, N., Ávila, J., Llorens-Martín, M., 2019. Adult hippocampal neurogenesis is abundant in neurologically healthy subjects and drops sharply in patients with Alzheimer's disease. Nat. Med. 25, 554—560.

Mota, S.I., Ferreira, I.L., Valero, J., Ferreiro, E., Carvalho, A.L., Oliveira, C.R., Rego, A.C., 2014. Impaired Src signaling and post-synaptic actin polymerization in Alzheimer's disease mice hippocampus - linking NMDA receptors and the reelin pathway. Exp. Neurol. 261, 698—709.

Oddo, S., Caccamo, A., Shepherd, J.D., Murphy, M.P., Golde, T.E., Kayed, R., Metherate, R., Mattson, M.P., Akbari, Y., LaFerla, F.M., 2003. Triple-transgenic model of Alzheimer's disease with plaques and tangles: intracellular Abeta and synaptic dysfunction. Neuron 39, 409—421.

Patzke, N., Spocter, M.A., Karlsson, K.Æ., Bertelsen, M.F., Haagensen, M., Chawana, R., Streicher, S., Kaswera, C., Gilissen, E., Alagaili, A.N., Mohammed, O.B., Reep, R.L., Bennett, N.C., Siegel, J.M., Ihunwo, A.O., Manger, P.R., 2015. In contrast to many other mammals, cetaceans have relatively small hippocampi that appear to lack adult neurogenesis. Brain Struct. Funct. 220, 361—383.

Paxinos, G., Franklin, K., 1997. The Mouse Brain in Stereotaxic Coordinates. Acad. Press.

Petreanu, L., Alvarez-Buylla, A., 2002. Maturation and death of adult-born olfactory bulb granule neurons: role of olfaction. J. Neurosci. 22, 6106—6113.

Piatti, V.C., Ewell, L.A., Leutgeb, J.K., 2013. Neurogenesis in the dentate gyrus: carrying the message or dictating the tone. Front Neurosci. 7, 50.

Plumpe, T., Ehninger, D., Steiner, B., Klempin, F., Jessberger, S., Brandt, M., Romer, B., Rodriguez, G.R., Kronenberg, G., Kempermann, G., 2006. Variability of doublecortin-associated dendrite maturation in adult hippocampal neurogenesis is independent of the regulation of precursor cell proliferation. BMC Neurosci. 7, 77.

Polito, L., Chierchia, A., Tunesi, M., Bouybayoune, I., Kehoe, P.G., Albani, D., Forloni, G., 2014. Environmental enrichment lessens cognitive decline in APP23 mice without affecting brain sirtuin expression. J. Alzheimers Dis. 42, 851—864.

Rodríguez-Iglesias, N., Sierra, A., Valero, J., 2019. Rewiring of memory circuits: connecting adult newborn neurons with the help of microglia. Front. Cell Dev. Biol. 7, 24.

Saxe, M.D., Battaglia, F., Wang, J.W., Malleret, G., David, D.J., Monckton, J.E., Garcia, A.D., Sofroniew, M.V., Kandel, E.R., Santarelli, L., Hen, R., Drew, M.R., 2006. Ablation of hippocampal neurogenesis impairs contextual fear conditioning and synaptic plasticity in the dentate gyrus. Proc. Natl. Acad. Sci. U S A. 103, 17501—17506.

Schindelin, J., Arganda-Carreras, I., Frise, E., Kaynig, V., Longair, M., Pietzsch, T., Preibisch, S., Rueden, C., Saalfeld, S., Schmid, B., Tinevez, J.Y., White, D.J., Hartenstein, V., Eliceiri, K., Tomancak, P., Cardona, A., 2012. Fiji: an open-source platform for biological-image analysis. Nat. Methods 9, 676—682.

Sebastiao, I., Candeias, E., Santos, M.S., de Oliveira, C.R., Moreira, P.I., Duarte, A.I., 2014. Insulin as a bridge between type 2 diabetes and Alzheimer disease—how anti-diabetics could be a solution for dementia. Front. Endocrinol. 5, 110.

Sorrells, S.F., Paredes, M.F., Cebrian-Silla, A., Sandoval, K., Qi, D., Kelley, K.W., James, D., Mayer, S., Chang, J., Auguste, K.I., Chang, E.F., Gutierrez, A.J., Kriegstein, A.R., Mathern, G.W., Oldham, M.C., Huang, E.J., Garcia-Verdugo, J.M., Yang, Z., Alvarez-Buylla, A., 2018. Human hippocampal neurogenesis drops sharply in children to undetectable levels in adults. Nature 555, 377—381.

Spalding, K.L., Bergmann, O., Alkass, K., Bernard, S., Salehpour, M., Huttner, H.B., Bostrom, E., Westerlund, I., Vial, C., Buchholz, B.A., Possnert, G., Mash, D.C., Druid, H., Frisen, J., 2013. Dynamics of hippocampal neurogenesis in adult humans. Cell 153, 1219—1227.

Stern, Y., 2009. Cognitive reserve. Neuropsychologia 47, 2015—2028.

Stranahan, A.M., Mattson, M.P., 2012. Metabolic reserve as a determinant of cognitive aging. J. Alzheimer's Dis. 30 (Suppl 2), S5—S13.

Sung, P.-S., Lin, P.-Y., Liu, C.-H., Su, H.-C., Tsai, K.-J., 2020. Neuroinflammation and neurogenesis in Alzheimer's disease and potential therapeutic approaches. Int. J. Mol. Sci. 21, 701—724.

Tiwari, S.K., Seth, B., Agarwal, S., Yadav, A., Karmakar, M., Gupta, S.K., Choubey, V., Sharma, A., Chaturvedi, R.K., 2015. Ethosuximide induces hippocampal neurogenesis and reverses cognitive deficits in an amyloid-β toxin-induced Alzheimer rat model via the phosphatidylinositol 3-kinase (PI3K)/Akt/Wnt/β-catenin pathway. J. Biol. Chem. 290, 28540—28558.

Toni, N., Teng, E.M., Bushong, E.A., Aimone, J.B., Zhao, C., Consiglio, A., Van Praag, H., Martone, M.E., Ellisman, M.H., Gage, F.H., 2007. Synapse formation on neurons born in the adult hippocampus. Nat. Neurosci. 10, 727—734.

Treit, D., Fundytus, M., 1988. Thigmotaxis as a test for anxiolytic activity in rats. Pharmacol. Biochem. Behav. 31, 959—962.

Valenta, T., Hausmann, G., Basler, K., 2012. The many faces and functions of beta-catenin. EMBO J. 31, 2714—2736.

Valero, J., España, J., Parra-Damas, A., Martín, E., Rodríguez-Álvarez, J., Saura, C.A., 2011. Short-term environmental enrichment rescues adult neurogenesis and memory deficits in APPSw,Ind transgenic mice. PLoS One 6, e16832.

Valero, J., Mastrella, G., Neiva, I., Sanchez, S., Malva, J.O., 2014. Long-term effects of an acute and systemic administration of LPS on adult neurogenesis and spatial memory. Front Neurosci. 8, 83.

Valero, J., Paris, I., Sierra, A., 2016. Lifestyle shapes the Dialogue between environment, microglia, and adult neurogenesis. ACS Chem. Neurosci. 7, 442—453.

Varela-Nallar, L., Inestrosa, N.C., 2013. Wnt signaling in the regulation of adult hippocampal neurogenesis. Front Cell Neurosci 7, 100.

Verret, L., Jankowsky, J.L., Xu, G.M., Borchelt, D.R., Rampon, C., 2007. Alzheimer's-type amyloidosis in transgenic mice impairs survival of newborn neurons derived from adult hippocampal neurogenesis. J. Neurosci. 27, 6771—6780.

Verret, L., Krezymon, A., Halley, H., Trouche, S., Zerwas, M., Lazouret, M., Lassalle, J.M., Rampon, C., 2013. Transient enriched housing before amyloidosis onset sustains cognitive improvement in Tg2576 mice. Neurobiol. Aging 34, 211—225.

Wang, R., Dineley, K.T., Sweatt, J.D., Zheng, H., 2004. Presenilin 1 familial Alzheimer's disease mutation leads to defective associative learning and impaired adult neurogenesis. Neuroscience 126, 305—312.

Wijesekara, N., Gonçalves, R.A., De Felice, F.G., Fraser, P.E., 2018. Impaired peripheral glucose homeostasis and Alzheimer's disease. Neuropharmacology 136, 172—181.

Wolfer, D.P., Madani, R., Valenti, P., Lipp, H.P., 2001. Extended analysis of path data from mutant mice using the public domain software Wintrack. Physiol. Behav. 73, 745—753.

Yu, X., Malenka, R.C., 2003. Beta-catenin is critical for dendritic morphogenesis. Nat. Neurosci. 6, 1169—1177.

Zainuddin, M.S.A., Thuret, S., 2012. Nutrition, adult hippocampal neurogenesis and mental health. Br. Med. Bull. 103, 89—114.

Zhang, Z., Hartmann, H., Do, V.M., Abramowski, D., Sturchler-Pierrat, C., Staufenbiel, M., Sommer, B., van de Wetering, M., Clevers, H., Saftig, P., De Strooper, B., He, X., Yankner, B.A., 1998. Destabilization of beta-catenin by mutations in presenilin-1 potentiates neuronal apoptosis. Nature 395, 698—702.